SIAM J. APPL. MATH.
Vol. 71, No. 4, pp. 1168–1203

FRACTIONAL CABLE EQUATION MODELS FOR ANOMALOUS ELECTRODIFFUSION IN NERVE CELLS: FINITE DOMAIN SOLUTIONS*

T. A. M. LANGLANDS†, B. I. HENRY‡, AND S. L. WEARNE§

Abstract. In recent work we introduced fractional Nernst–Planck equations and related fractional cable equations to model electrodiffusion of ions in nerve cells with anomalous subdiffusion along and across the nerve cells. This work was motivated by many computational and experimental studies showing that anomalous diffusion is ubiquitous in biological systems with binding, crowding, or trapping. For example, recent experiments have shown that anomalous subdiffusion occurs along the axial direction in spiny dendrites due to trapping by the spines. We modeled the subdiffusion in two ways leading to two fractional cable equations and presented fundamental solutions on infinite and semi-infinite domains. Here we present solutions on finite domains for mixed Robin boundary conditions. The finite domain solutions model passive electrotonic properties of spiny dendritic branch segments with ends that are voltage clamped, sealed, or killed. The behavior of the finite domain solutions is similar for both fractional cable equations. With uniform subdiffusion along and across the nerve cells, the solution approaches the standard nonzero steady state, but the approach is slowed by the anomalous subdiffusion. If the subdiffusion is more anomalous along the axial direction, then (boundary conditions permitting) the solution converges to a zero steady state, whereas if the subdiffusion is less anomalous along the axial direction, then the solution approaches a spatially linear steady state. These solutions could be compared with realistic electrophysiological experiments on actual dendrites.

Key words. neuron, cable equation, anomalous diffusion, fractional derivative

AMS subject classifications. 92C20, 35R11, 26A33, 60J60, 33E12, 35Q84, 60G22, 44A10

DOI. 10.1137/090775920

1. Introduction.

The cable equation

$$c_m \frac{\partial V_m}{\partial t} = \frac{d}{4r_L} \frac{\partial^2 V_m}{\partial x^2} - i_m + i_e \tag{1.1}$$

and related theory underpin much of computational neuroscience [15] as the basic macroscopic model for electrophysiological behaviors in neuronal processes such as axons, dendrites, and dendritic trees [26]. The spatio-temporal behavior of the membrane potential V_m along a dendrite of diameter d is modeled by solving the cable equation on a finite domain, with suitable boundary conditions. The variable i_m in this equation models the total ionic transmembrane current density, which is specified separately using Ohm's law for passive cables or Hodgkin–Huxley equations for active cables. The injected current density i_e is prescribed by experiment, but the purported electrical properties of the dendrite (the membrane capacitance per unit surface area c_m and the axial resistivity r_L) are parameters found by fitting cable

*Received by the editors November 3, 2009; accepted for publication (in revised form) May 4, 2011; published electronically July 21, 2011. This research was supported by the Australian Commonwealth Government ARC Discovery Grants Scheme and NIH grant MH071818.

http://www.siam.org/journals/siap/71-4/77592.html

†Department of Mathematics and Computing, Faculty of Science, University of Southern Queensland, Toowoomba QLD 4250, Australia (Trevor.Langlands@usq.edu.au).

‡Department of Applied Mathematics, School of Mathematics and Statistics, University of New South Wales, Sydney NSW 2052, Australia (B.Henry@unsw.edu.au).

§This author is deceased. Former address: Biomathematics Laboratory, Department of Neuroscience, Mount Sinai School of Medicine, New York, NY 10029-6574.

solutions to experimental measurements. In the passive cable equation the transmembrane current density from Ohm's law is defined by

$$i_m = \frac{V_m - V_{rest}}{r_m}, \tag{1.2}$$

which introduces the specific membrane resistance r_m as an additional parameter to be fit to experimental measurements. If there is no external injected current ($i_e = 0$), then the cable model reduces to a two parameter fit in terms of the space constant $\lambda = \sqrt{dr_m/4r_L}$, measuring the distance over which the steady state voltage attenuates by a factor $1/e$, and the time constant $\tau = r_m c_m$, measuring the time for the homogeneous voltage on a membrane patch to decay by a factor $1/e$.

At a fundamental level the electrophysiological behaviors in neuronal processes emerge from the electrodiffusion of ions across and along the nerve cell membrane. The standard model for electrodiffusion of ions is the Nernst–Planck equation, which in the case of an axially symmetric cylindrical geometry is given by [25]

$$\frac{\partial C_k}{\partial t} = D_k \frac{\partial^2 C_k}{\partial x^2} + D_k \frac{F z_k}{RT} \frac{\partial}{\partial x}\left(C_k \frac{\partial V_m}{\partial x}\right) - \frac{4}{dF z_k} i_{m,k}. \tag{1.3}$$

In this equation C_k denotes the concentration of ionic species k with charge z_k and diffusivity D_k. Definitions of the all quantities and units involved in this equation are provided in Table 1.1.

TABLE 1.1
Definitions and units for quantities in the cable equation and the Nernst–Planck equation.

Quantity	Definition	Units
V_m	membrane voltage	V
x	distance	μm
t	time	s
i_m	transmembrane current per unit area	A μm^{-2}
i_e	injected current per unit area	A μm^{-2}
c_m	membrane capacitance per unit surface area	F μm^{-2}
r_L	axial resistivity	$\Omega\,\mu$m
r_m	specific membrane resistance	$\Omega\,\mu$m^2
C_k	concentration	moles μm^{-2}
T	temperature	K
F	Faraday's constant	C mole^{-1}
R	universal gas constant	J K^{-1} mole^{-1}
z_k	valence	
d	cable diameter	μm
D_k	diffusivity	μm^2 s^{-1}
r_L	longitudinal resistivity	$\Omega\,\mu$m
$D(\gamma)$	generalized diffusivity	μm^2 s$^{-\gamma}$
$r_L(\gamma)$	generalized longitudinal resistivity	$\Omega\,\mu$m s$^{\gamma-1}$

The first term on the right-hand side of (1.3) models random Brownian motion, and the second term models drift due to the electric field associated with the membrane potential. The cable equation (1.1) can be derived from the Nernst–Planck equation (1.3) by considering slowly varying ionic concentrations along the axial direction, $\partial C_k/\partial x \approx 0$, and identifying [25]

$$V_m(x,t) = V_{rest} + \frac{Fd}{4c_m} \sum_k z_k (C_k(x,t) - C_{k,rest}), \tag{1.4}$$

$$\frac{1}{r_L} = \frac{F^2}{RT}\sum_k z_k^2 D_k C_k, \tag{1.5}$$

and $i_m = \sum_k i_{m,k}$. Two points of note are (i) $Fd/4c_m$ is sufficiently large that $\partial V_m/\partial x$ is not negligible in (1.4), and (ii) the diffusivity D_k impacts the resistivity r_L in (1.5) and not just the diffusion. This latter point is important because it shows how alterations in diffusion can affect electrical properties of the cable.

The cable equation thus represents a model for electrical properties of a spatially homogeneous cylindrical cable with ionic motions driven by concentration gradients (standard diffusion) and driven by the electric field of the membrane potential (which is also dependent on ionic concentrations). The underlying assumption of spatial homogeneity, however, is not well supported by observations of neuroanatomy and should be revised in light of our vastly increased understanding of processes at the molecular level in neuronal cytoplasm and membrane. Even in the early sketches of individual neurons by Santiago Ramón Cajal more than 100 years ago it was apparent that dendritic branches are not spatially homogeneous cylinders. The irregularities are particularly profound at the micrometer scale of spiny protrusions that decorate most dendrites. The plasticity of these dendritic spines and their central role in learning and memory is the subject of cutting-edge research into mechanisms of synaptic plasticity (see, e.g., [3]). One of the major motivations for our study is to provide a detailed understanding of how spines impact the spatio-temporal properties of the passive cell membrane potential. A recent study of interest in this connection [28] has reported that the density and morphology of dendritic spines significantly alters the diffusion of molecules through the cytoplasm of Purkinje cell dendrites. Other heterogeneous irregularities at the micrometer and submicron scale associated with macromolecular crowding, binding, trapping, and buffering also impact the diffusion of ions and other molecules [11, 32, 40, 2]. On macroscopic scales the effect of such obstacles is to slow the diffusive motion of the ions relative to free diffusion in aqueous media (see also [29, 30, 31, 37]). A key signature of the anomalously slow diffusion is sublinear power law scaling of the diffusive spatial variance in time. Similar anomalous subdiffusion has been reported in numerous other biological studies [8, 33, 34, 35, 5, 2, 27].

Anomalous subdiffusion can be modeled using a modified diffusion equation

$$\frac{\partial C}{\partial t} = \mathcal{D}(\gamma, t)\nabla^2 C \tag{1.6}$$

with the diffusion constant replaced by a fractional temporal operator. Two possibilities for this operator are the fractional Brownian motion (fBm) model [39, 38]

$$\mathcal{D}_I(\gamma, t) = D(\gamma)\gamma t^{\gamma-1} \tag{1.7}$$

or the power law waiting time continuous time random walk (CTRW) model [20, 19]

$$\mathcal{D}_{II}(\gamma, t) = D(\gamma)\frac{\partial^{1-\gamma}}{\partial t^{1-\gamma}}, \tag{1.8}$$

where $D(\gamma)$ is a generalized diffusion coefficient with units of $m^2 s^{-\gamma}$ and

$$\frac{\partial^{1-\gamma}}{\partial t^{1-\gamma}}Y(t) = \frac{1}{\Gamma(\gamma)}\frac{\partial}{\partial t}\int_0^t \frac{Y(t')}{(t-t')^{1-\gamma}}dt' \tag{1.9}$$

defines the Riemann–Liouville fractional derivative of order $1-\gamma$. Both fractional diffusion models yield the same sublinear power law spatial variance, but the fundamental solutions are different with different long time asymptotic behavior. One

possibility for modeling anomalous electrodiffusion of ions is to use a modified Nernst–Planck equation with the diffusion constant replaced by an fBm or CTRW fractional temporal operator. We considered this approach in a recent model for electrodiffusion in spiny dendrites [14], and we found that subdiffusion associated with changes in spine densities impacts both the speed and amplitude of postsynaptic potentials propagating along spiny dendrites. In a related study, Fedotov and Méndez [9] considered separate equations for the populations of particles inside spines and for the populations of particles inside dendrites. Their work clearly demonstrated how anomalous subdiffusion arises from power law trapping times in the spines.

In recent research [14, 17] we derived fractional cable equations

$$c_m \frac{\partial V_m}{\partial t} = \frac{\mathcal{D}(\gamma,t)}{D(\gamma)} \left(\frac{d}{4r_L(\gamma)} \frac{\partial^2 V_m}{\partial x^2} \right) - i_m \tag{1.10}$$

from fractional Nernst–Planck equations with the diffusion constant replaced by an fBm or CTRW fractional temporal operator and with the modified longitudinal resistivity $r_L(\gamma)$ defined by

$$\frac{1}{r_L} = \frac{F^2}{RT} \sum_k z_k^2 D_k(\gamma) C_k \tag{1.11}$$

and the anomalous diffusion scaling exponent $\gamma \approx \gamma_k$ taken to be similar for all mobile ions. The fractional cable equations are consistent with a fractional axial current density

$$i_L = -\frac{\mathcal{D}(\gamma,t)}{D(\gamma)} \left(\frac{1}{r_L(\gamma)} \frac{\partial V_m}{\partial x} \right). \tag{1.12}$$

Retarded diffusion has also been reported across ion channels [10], and to allow for the possibility that this diffusion is also anomalous we introduce a fractional transmembrane current density by defining

$$i_m = \frac{\mathcal{D}(\kappa,t)}{D(\kappa)} \left(\frac{V_m - V_{rest}}{r_m} \right). \tag{1.13}$$

We note that a nonzero steady state solution cannot be possible unless the scaling exponents γ and κ, which characterize the anomalous diffusion along the dendrite and across the membrane, respectively, are equal. The current equations (1.12), (1.13) are a fractional (or nonlocal variant) of Ohm's law. Fedotov and Méndez [9] reported a similar nonlocal flux in their two species model for diffusion in spiny dendrites.

Using (1.13) together with the dimensionless variables

$$T = t/\tau_m, \tag{1.14}$$

$$X = x\tau_m^{\frac{1-\gamma}{2}} / \sqrt{\frac{dr_m}{4r_L}}, \tag{1.15}$$

$$\mu^2 = \tau_m^{\kappa-1}, \tag{1.16}$$

and $V = V_m - V_{rest}$, the fractional linear cable equations can be written as

$$\text{Model I} \qquad \begin{aligned} \frac{\partial V}{\partial T} &= \gamma T^{\gamma-1} \left(\frac{\partial^2 V}{\partial X^2} \right) - \mu^2 \kappa T^{\kappa-1} (V) \\ &= \gamma T^{\gamma-1} \left(\frac{\partial^2 V}{\partial X^2} - \mu^2 \frac{\kappa}{\gamma} T^{\kappa-\gamma} V \right), \end{aligned} \tag{1.17}$$

based on the fBm model, and

$$\text{Model II} \qquad \frac{\partial V}{\partial T} = \frac{\partial^{1-\gamma}}{\partial T^{1-\gamma}}\left(\frac{\partial^2 V}{\partial X^2}\right) - \mu^2 \frac{\partial^{1-\kappa}}{\partial T^{1-\kappa}}(V), \tag{1.18}$$

based on the CTRW model. The standard cable equation is recovered in each case by setting $\gamma = \kappa = \mu^2 = 1$. The solutions of the fractional cable equations provide approximations for passive electrotonic properties of spiny dendrites that could be compared with experiments [14].

In an earlier paper [17] we derived fundamental solutions of the fractional cable equations, (1.17) and (1.18), on infinite domains and semi-infinite domains, and we derived results for action potential firing rates based on simple integrate and fire models with an external injected current. In this paper we have extended these results by deriving analytic solutions to fractional cable equation models on finite domains for general mixed Robin boundary conditions. The simplest boundary conditions to impose on a finite cable at an end $X = a$ are [36] (i) voltage clamped (Dirichlet), $V(a,T) = b \neq 0$, (ii) sealed (von Neumann), $\partial V(a,T)/\partial X = 0$, and (iii) killed (Dirichlet), $V(a,T) = 0$. In the following we consider mixed Robin boundary conditions of the form

$$a_o \frac{\partial V(0,T)}{\partial X} + b_o V(0,T) = g_o, \quad a_L \frac{\partial V(L,T)}{\partial X} + b_L V(L,T) = g_L, \tag{1.19}$$

with a_o, b_o, g_o, a_L, b_L, and g_L specified constants. These general boundary conditions allow for all possibilities of voltage clamped, sealed, and killed on one or both ends of the domain. We note that the pair a_o and b_o, and likewise the pair a_L and b_L, cannot both be set to zero. Our consideration of the general case of inhomogeneous Robin boundary conditions is essentially mathematically motivated, giving us flexibility in dealing with various combinations of von Neumann and Dirichlet conditions, and enabling possible applications of fractional cable equations in broader contexts. In related work, the time-fractional diffusion equation was solved for absorbing and reflecting boundaries using the method of images and separation of variables in [19]. The time-fractional diffusion equation with partially absorbing and partially reflecting boundaries, corresponding to homogeneous Robin boundary conditions ($g_0 = g_L = 0$), was considered in [7, 12]. Numerical methods for solving the fractional cable equation on finite domains with nonhomogeneous Dirichlet boundary conditions were considered very recently in [18].

The remainder of this paper is organized as follows. In section 2 we present solutions for $\gamma = \kappa$. In section 3 we consider the model equations for $\gamma \neq \kappa$. We begin by carrying out temporal Laplace transforms of the model equations and boundary conditions, and we find the solutions in Laplace space. In section 4 we present the general solutions for $\gamma \neq \kappa$ after inverse Laplace transforms have been carried out. In section 5 we compare representative model solutions for fractional cable equations based on the fBm model and the CTRW model for special cases of the boundary conditions. The solutions are plotted at different times, and the long time behavior inferred from these plots is compared with asymptotic long time behaviors of the model solutions. We conclude with a summary and discussion in section 6. Supplementary material, including short and long time asymptotics, and explicit verification of the solutions are given in the appendices.

2. Solutions for $\gamma = \kappa$ case. In the case that $\gamma = \kappa$ both (1.17) and (1.18) can be factored as

$$\frac{\partial V}{\partial T} = \tau(T;\gamma)\left(\frac{\partial^2}{\partial X^2} - \mu^2\right)V, \tag{2.1}$$

where the operator

$$\tau(T;\gamma) = \begin{cases} \gamma T^{\gamma-1} & \text{Model I,} \\ \frac{\partial^{1-\gamma}}{\partial T^{1-\gamma}} & \text{Model II.} \end{cases} \tag{2.2}$$

The solution can thus be written as

$$V(X,T) = \psi(X;\mu) + \tilde{V}(X,T), \tag{2.3}$$

where

$$\psi(X;\mu) = g_o \frac{a_L\mu\cosh\mu(L-X) + b_L\sinh\mu(L-X)}{(b_o b_L - a_o a_L\mu^2)\sinh\mu L + (b_o a_L - a_o b_L)\mu\cosh\mu L} + g_L \frac{b_o\sinh\mu X - a_o\mu\cosh\mu X}{(b_o b_L - a_o a_L\mu^2)\sinh\mu L + (b_o a_L - a_o b_L)\mu\cosh\mu L} \tag{2.4}$$

is the ($\gamma = \kappa$) hyperbolic steady state solution that satisfies the homogeneous equation

$$\frac{d^2\psi}{dX^2} - \mu^2\psi = 0, \tag{2.5}$$

together with the inhomogeneous boundary conditions

$$a_o\frac{d\psi(0)}{dX} + b_o\psi(0) = g_o, \qquad a_L\frac{d\psi(L)}{dX} + b_L\psi(L) = g_L, \tag{2.6}$$

and $\tilde{V}(X,T)$ satisfies (2.1) together with homogeneous Robin boundary conditions ((1.19) with $g_0 = g_L = 0$).

The solution $\tilde{V}$ can be found using separation of variables. Assuming a separable solution $\tilde{V} = \Psi(X)\Phi(T)$ in (2.1) yields

$$\frac{d\Phi}{dT} = \lambda\tau(T)\Phi(T) \tag{2.7}$$

and

$$\frac{d^2\Psi}{dX^2} - \mu^2\Psi = \lambda\Psi, \tag{2.8}$$

where λ is the separation constant. After applying the homogeneous Robin boundary conditions to the separable solution we find the boundary conditions for $\Psi(X)$ as follows:

$$a_o\frac{d\Psi(0)}{dX} + b_o\Psi(0) = 0, \qquad a_L\frac{d\Psi(L)}{dX} + b_L\Psi(L) = 0. \tag{2.9}$$

In general the boundary value problem defined by (2.8) and (2.9) may have finitely many positive eigenvalues (for certain choices of the constants a_0, a_L, b_0, b_L, L) and

infinitely many negative eigenvalues. In the following we restrict our consideration to cases with strictly negative eigenvalues

$$\lambda = -\lambda_n^2 - \mu^2, \quad n = 0, 1, 2 \ldots.$$

This includes the following special cases: (i) $a_0 = a_L = 0$ with $\lambda_n = n\pi/L$, (ii) $b_0 = b_L = 0$ with $\lambda_n = n\pi/L$, (iii) $a_L = b_L$, $a_0 = b_0$ with $\lambda_n = n\pi/L$, (iv) $a_L = a_0$, $b_L = b_0$ with $\lambda_n = n\pi/L$, (v) $a_0 = b_L = 0$ with $\lambda_n = (2n-1)\pi/L$, (vi) $a_L = b_0 = 0$ with $\lambda_n = (2n-1)\pi/L$.

It is a simple matter to solve (2.7) for each of the model operators in (2.2). This then results in the final solution

$$V(X,T) = \psi(X;\mu) + \sum_{n=0}^{\infty} c_n \Psi_n(X) \Phi_n(T), \tag{2.10}$$

where

$$\Phi_n(T) = \begin{cases} e^{-(\lambda_n^2+\mu^2)T^\gamma} & \text{Model I,} \\ \\ E_\gamma\left(-(\lambda_n^2+\mu^2)T^\gamma\right) & \text{Model II.} \end{cases} \tag{2.11}$$

In the above solution $E_\alpha(z)$ is a Mittag–Leffler function (see Appendix B), and $\Psi_n(X)$ are the eigenfunctions of the boundary value problem defined by

$$\frac{d^2\Psi_n}{dX^2} + \lambda_n^2 \Psi_n = 0 \tag{2.12}$$

together with (2.9). Here and elsewhere in this paper we have assumed that the initial condition can be written in the form

$$V(X,0) = \psi(X;\mu) + \sum_{n=0}^{\infty} c_n \Psi_n(X). \tag{2.13}$$

Note that when $\gamma = \kappa = 1$ both model solutions reduce to the standard solution

$$V(X,T) = \psi(X;\mu) + \sum_{n=0}^{\infty} c_n \Psi_n(X) \exp\left(-(\lambda_n^2+\mu^2)T\right). \tag{2.14}$$

The effect of reducing $\gamma = \kappa < 1$ results in a faster initial attenuation but a slower long time attenuation. The attenuation is slower in Model II than in Model I due to the stretched exponential nature of the Mittag–Leffler function.

In the subsequent sections we use Laplace transform methods to obtain solutions of Model I and Model II for nonhomogeneous Robin boundary conditions and nonequal γ and κ. These solutions reduce to the solutions in this section when $\gamma = \kappa$.

3. Solutions for $\gamma \neq \kappa$ case. In this section we find the finite domain solutions in Laplace space when $\gamma \neq \kappa$. For Model II this entails a straightforward Laplace transform of the governing equation of (1.18) and the boundary conditions (1.19) with respect to the variable T. For Model I we first perform a change of variable $U = T^\gamma$ transforming (1.17) into the standard diffusion equation with U now playing the role of the time. With this change of variables, the boundary conditions (1.19) become explicitly time-dependent, and we perform a Laplace transform of both the evolution equation and the boundary conditions with respect to U.

Before proceeding with this we note that when $\gamma \neq \kappa$ the governing equations (1.18) and (1.17) do not admit a nonzero steady state solution $V = V(X)$. A nonzero steady state would have to satisfy $V_{XX} = \mu^2 \tau^{-1}(T;\gamma)\left[\tau(T;\kappa)\left(V(X)\right)\right]$ for all X and T, but the left-hand side is independent of time, and the right-hand side is time-dependent if $\gamma \neq \kappa$. On the other hand the long time asymptotic behavior may approach the zero steady state $V = 0$ or the nonzero linear steady state $V = c_1 X + c_2$. In this latter case the left-hand side is identically zero, and the right-hand side approaches zero as $T \to \infty$ if $\gamma > \kappa$.

3.1. Model I. The solution of (1.17) can be written as

$$V(X,T) = \mathrm{e}^{-\mu^2 T^{\kappa}} W(X,U), \tag{3.1}$$

where

$$U = T^{\gamma} \tag{3.2}$$

and

$$\frac{\partial W}{\partial U} = \frac{\partial^2 W}{\partial X^2} \tag{3.3}$$

with initial condition $W(X,0) = V(X,0)$. The corresponding mixed boundary conditions for $W(X,U)$ become

$$a_o \frac{\partial W(0,U)}{\partial X} + b_o W(0,U) = g_o \,\mathrm{e}^{\mu^2 U^{\theta}}, \qquad a_L \frac{\partial W(L,U)}{\partial X} + b_L W(L,U) = g_L \,\mathrm{e}^{\mu^2 U^{\theta}}, \tag{3.4}$$

where $\theta = \kappa/\gamma$. The mixed Robin boundary conditions are explicitly time-dependent (U-dependent) here.

The Laplace transform of (3.3) with respect to the variable U leads to

$$\frac{\partial^2 \widehat{W}}{\partial X^2} - \lambda^2(s)\widehat{W} = -V(X,0), \tag{3.5}$$

where

$$\lambda^2(s) = s \tag{3.6}$$

and s is the Laplace variable. The Laplace transforms of the boundary conditions (3.4) yield

$$a_o \frac{\partial \widehat{W}(0,s)}{\partial X} + b_o \widehat{W}(0,s) = g_o \widehat{P}_{\theta}(s), \qquad a_L \frac{\partial \widehat{W}(L,s)}{\partial x} + b_L \widehat{W}(L,s) = g_L \widehat{P}_{\theta}(s), \tag{3.7}$$

where

$$\widehat{P}_{\theta}(s) = \mathcal{L}\left\{\mathrm{e}^{\mu^2 U^{\theta}}\right\}(s), \tag{3.8}$$

where $\mathcal{L}\{\}(()\,s)$ denotes the Laplace operator. It is straightforward (see Appendix C) to obtain the Laplace space solution $\widehat{W}(X,s)$ of (3.5) for the given boundary conditions. This yields (3.7),

$$\widehat{W}(X,s) = \left(\widehat{P}_{\theta}(s) - \frac{1}{\lambda^2(s) - \mu^2}\right)\psi(X;\lambda(s)) + \frac{\psi(X;\mu)}{\lambda^2(s) - \mu^2} + \sum_{n=0}^{\infty} \frac{c_n \Psi_n(X)}{\lambda^2(s) + \lambda_n^2}, \tag{3.9}$$

where $\psi(X;\lambda(s))$ and $\psi_n(X)$ are solutions of (2.5) (with boundary conditions (2.6)) and (2.12) (with boundary conditions (2.9)), respectively.

3.2. Model II. For Model II we proceed by first taking the Laplace transform of the governing equation (1.18),

$$s\widehat{V}(X,s) - V(X,0) = s^{1-\gamma}\frac{\partial^2\widehat{V}(X,s)}{\partial X^2} - \left[\frac{\partial^{-\gamma}}{\partial T^{-\gamma}}\frac{\partial^2 V(X,T)}{\partial X^2}\right|_{T=0} - \mu^2\left(s^{1-\kappa}\widehat{V}(X,s) - \left[\frac{\partial^{-\kappa}}{\partial T^{-\kappa}}V(X,T)\right|_{T=0}\right), \tag{3.10}$$

where s is the Laplace variable and we have denoted the Laplace transformed function with a hat. This equation can be rearranged to arrive at

$$\frac{\partial^2\widehat{V}(X,s)}{\partial X^2} - \lambda^2(s)\widehat{V}(X,s) = -s^{\gamma-1}V(X,0), \tag{3.11}$$

where

$$\lambda^2(s) = s^\gamma + \mu^2 s^{\gamma-\kappa}, \tag{3.12}$$

and we have used the result that the fractional integrals evaluated at time zero are zero (see Appendix A).

The Laplace transform of the boundary conditions in (1.19) yields

$$a_o\frac{\partial\widehat{V}(0,s)}{\partial X} + b_o\widehat{V}(0,s) = \frac{g_o}{s}, \qquad a_L\frac{\partial\widehat{V}(L,s)}{\partial X} + b_L\widehat{V}(L,s) = \frac{g_L}{s}, \tag{3.13}$$

and the solution of (3.11) with these boundary conditions is (see Appendix C)

$$\widehat{V}(X,s) = \left(\frac{1}{s} - \frac{s^{\gamma-1}}{\lambda^2(s)-\mu^2}\right)\psi(X;\lambda(s)) + \frac{s^{\gamma-1}}{\lambda^2(s)-\mu^2}\psi(X;\mu) + \sum_{n=0}^{\infty}\frac{s^{\gamma-1}}{\lambda^2(s)+\lambda_n^2}c_n\Psi_n(X). \tag{3.14}$$

4. General solutions. To find the solution for both models we need to invert the Laplace transforms in (3.9) and (3.14). This can be facilitated by first expanding the difference $\psi(X;\lambda(s)) - \psi(X;\mu)$ for $0 \le X \le L$ in terms of the eigenfunctions, $\Psi_n(X)$, as follows:

$$\psi(X;\lambda(s)) - \psi(X;\mu) = \sum_{n=0}^{\infty} d_n\left(\frac{1}{\lambda^2(s)+\lambda_n^2} - \frac{1}{\mu^2+\lambda_n^2}\right)\Psi_n(X), \tag{4.1}$$

where

$$d_n = \frac{\rho_n}{\|\Psi_n\|^2} = \frac{\rho_n}{\int_0^L (\Psi_n(X))^2\,dX} \tag{4.2}$$

with

$$\rho_n = \begin{cases} \frac{X_n(L)g_L}{a_L} - \frac{X_n(0)g_o}{a_o} & \text{if} \quad a_o \neq 0 \quad \text{and} \quad a_L \neq 0, \\ \frac{X_n(L)g_L}{a_L} + \frac{X_n'(0)g_o}{b_o} & \text{if} \quad a_o = 0 \quad \text{and} \quad a_L \neq 0, \\ -\frac{X_n'(L)g_L}{b_L} - \frac{X_n(0)g_o}{a_o} & \text{if} \quad a_o \neq 0 \quad \text{and} \quad a_L = 0, \\ -\frac{X_n'(L)g_L}{b_L} + \frac{X_n'(0)g_o}{b_o} & \text{if} \quad a_o = 0 \quad \text{and} \quad a_L = 0. \end{cases} \tag{4.3}$$

The appropriate choices for the parameters a_o, a_L, b_o, b_L, g_o, and g_L are defined by the boundary conditions in (1.19).

4.1. Model I. After substituting (4.1) into (3.9) we can write

$$\widehat{W}(X,s) = \psi(X;\mu)\widehat{P}_\theta(s) + \sum_{n=0}^{\infty}\left[c_n\widehat{A}_n^*(s) + d_n\widehat{B}_n^*(s)\right]\Psi_n(X), \tag{4.4}$$

where

$$\widehat{A}_n^*(s) = \frac{1}{\lambda^2(s)+\lambda_n^2} = \frac{1}{s+\lambda_n^2} \tag{4.5}$$

and

$$\widehat{B}_n^*(s) = \frac{1}{\lambda_n^2+\mu^2}\left(\widehat{A}_n^*(s) - \widehat{P}_\theta(s)\right) + \widehat{P}_\theta(s)\widehat{A}_n^*(s). \tag{4.6}$$

Using (3.1), we can now write

$$V(X,T) = \sum_{n=0}^{\infty}\left[c_nA_n(T) + d_nB_n(T)\right]\Psi_n(X) + \psi(X;\mu), \tag{4.7}$$

where

$$A_n(T) = \mathrm{e}^{-\mu^2T^\kappa}A_n^*(T^\gamma), \tag{4.8}$$

$$B_n(T) = \mathrm{e}^{-\mu^2T^\kappa}B_n^*(T^\gamma), \tag{4.9}$$

and it remains to find the explicit expressions for the Laplace inversions of $\widehat{A}_n^*(s)$ and $\widehat{B}_n^*(s)$.

The transform (4.5) can be readily inverted,

$$A_n^*(T) = \mathrm{e}^{-\lambda_n^2T}, \tag{4.10}$$

so that

$$A_n(T) = \mathrm{e}^{-\mu^2T^\kappa-\lambda_n^2T^\gamma}. \tag{4.11}$$

The transform (4.6) can be inverted by first expanding P_θ as a Taylor series and then inverting term by term (see Appendix D). This results in

$$\begin{aligned} B_n^*(T) = {} & \left(\frac{1}{\lambda_n^2} - \frac{1}{\lambda_n^2+\mu^2}\right)\left(P_\theta(T) - A_n^*(T)\right) \\ & - \frac{1}{\lambda_n^2}\sum_{m=1}^{\infty}\frac{\left(\mu^2T^\theta\right)^m}{m!}\Gamma\left(1+\theta m\right)E_{1,1+\theta m}\left(-\lambda_n^2T\right), \qquad n>0, \end{aligned} \tag{4.12}$$

where $E_{\alpha,\beta}(z)$ is the Mittag–Leffler function given in (B.1) [24]. In the case $n=0$ the result is

$$B_0^*(T) = \frac{1}{\mu^2}\left(1-P_\theta(T)\right) + \tau\ {}_1F_1\left(\frac{1}{\theta};1+\frac{1}{\theta};\mu^2T^\theta\right), \tag{4.13}$$

where ${}_1F_1\left(a;b;z\right)$ is the confluent hypergeometric function of the first kind (Chap. 13 in [1]). It now follows from (4.9) that

$$B_n(T) = \left(\frac{1}{\lambda_n^2} - \frac{1}{\lambda_n^2+\mu^2}\right)\left(1-A_n(T)\right) - \frac{\mathrm{e}^{-\mu^2 t^\kappa}}{\lambda_n^2}\sum_{m=1}^{\infty}\frac{\left(\mu^2 T^\kappa\right)^m}{m!}\Gamma\left(1+\frac{\kappa}{\gamma}m\right)E_{1,1+\frac{\kappa}{\gamma}m}\left(-\lambda_n^2 T^\gamma\right), \qquad n>0, \tag{4.14}$$

and

$$B_0(T) = -\frac{1}{\mu^2}\left(1-\mathrm{e}^{-\mu^2 T^\kappa}\right) + T^\gamma \mathrm{e}^{-\mu^2 T^\kappa}\,{}_1F_1\left(\frac{\gamma}{\kappa};1+\frac{\gamma}{\kappa};\mu^2 T^\kappa\right). \tag{4.15}$$

We also note that, with the identity [1]

$$\mathrm{e}^x\,{}_1F_1\left(a;b;-x\right) = {}_1F_1\left(b-a;b;x\right), \tag{4.16}$$

we can write

$$B_0(T) = -\frac{1}{\mu^2}\left(1-\mathrm{e}^{-\mu^2 T^\kappa}\right) + T^\gamma\,{}_1F_1\left(1;1+\frac{\gamma}{\kappa};-\mu^2 T^\kappa\right), \tag{4.17}$$

and then using (B.5)

$$B_0(T) = -\frac{1}{\mu^2}\left(1-\mathrm{e}^{-\mu^2 T^\kappa}\right) + T^\gamma\Gamma\left(1+\frac{\gamma}{\kappa}\right)E_{1,1+\frac{\gamma}{\kappa}}\left(-\mu^2 T^\kappa\right). \tag{4.18}$$

4.2. Model II. In a similar manner to Model I we find, with the aid of (4.1), that the solutions in (3.14) can be written as

$$\widehat{V}(X,s) = \sum_{n=0}^{\infty}\left[c_n\widehat{A}_n(s) + d_n\widehat{B}_n(s)\right]\Psi_n(X) + \frac{\psi(X;\mu)}{s}, \tag{4.19}$$

where

$$\widehat{A}_n(s) = \frac{s^{\gamma-1}}{\lambda^2(s)+\lambda_n^2} = \frac{1}{s+\lambda_n^2 s^{1-\gamma}+\mu^2 s^{1-\kappa}} \tag{4.20}$$

and

$$\widehat{B}_n(s) = \frac{\mu^2}{\lambda_n^2+\mu^2}\left(s^{-\gamma}-s^{-\kappa}\right)\widehat{A}_n(s). \tag{4.21}$$

Note that if $\lambda_n \neq 0$, then we can write

$$\widehat{B}_n(s) = \frac{\mu^2}{\lambda_n^2(\lambda_n^2+\mu^2)}\left(\frac{1}{s}-\widehat{A}_n(s)\right) - \frac{\mu^2}{\lambda_n^2}s^{-\kappa}\widehat{A}_n(s). \tag{4.22}$$

After inverting the Laplace transform in (4.19), the solution can be written as

$$V(X,T) = \psi(X;\mu) + \sum_{n=0}^{\infty}\left[c_n A_n(T) + d_n B_n(T)\right]\Psi_n(X), \tag{4.23}$$

where $B_n(T)$ and $A_n(T)$ are to be found by inverting $\widehat{B}_n(s)$ and $\widehat{A}_n(s)$, respectively.

First we consider the inversion of $\widehat{A}_n(s)$. Here we follow the procedure in [13, 24, 16] and rewrite (4.20) as

$$\widehat{A}_n(s) = \frac{s^{\gamma-1}}{s^\gamma + \lambda_n^2} \frac{1}{1 + \dfrac{\mu^2 s^{\gamma-\kappa}}{s^\gamma + \lambda_n^2}} = \sum_{m=0}^{\infty} \frac{\left(-\mu^2\right)^m}{m!} \frac{m!\; s^{\gamma-(1+(\kappa-\gamma)m)}}{\left(s^\gamma + \lambda_n^2\right)^{m+1}}. \tag{4.24}$$

Now from (B.2), we can identify each term in this series as a Mittag–Leffler function which can be inverted, term by term, to arrive at

$$A_n(T) = \sum_{m=0}^{\infty} \frac{\left(-\mu^2 T^\kappa\right)^m}{m!} E^{(m)}_{\gamma,1+(\kappa-\gamma)m}\left(-\lambda_n^2 T^\gamma\right). \tag{4.25}$$

When $n = 0$, this simplifies to

$$A_0(T) = E_{\kappa,1}\left(-\mu^2 T^\kappa\right). \tag{4.26}$$

Using the transform properties of fractional integrals [24], we can write

$$B_n(T) = \frac{\mu^2}{\lambda_n^2\left(\lambda_n^2 + \mu^2\right)}\left[1 - A_n(T)\right] - \frac{\mu^2}{\lambda_n^2} \frac{d^{-\kappa} A_n(T)}{dT^{-\kappa}}, \tag{4.27}$$

and when $n = 0$,

$$B_0(T) = \frac{d^{-\gamma} A_0(T)}{dT^{-\gamma}} - \frac{d^{-\kappa} A_0(T)}{dT^{-\kappa}}. \tag{4.28}$$

After evaluating the fractional integrals of the Mittag–Leffler functions, we have

$$B_n(T) = \frac{\mu^2}{\lambda_n^2\left(\lambda_n^2 + \mu^2\right)}\left[1 - A_n(T)\right] - \frac{\mu^2 T^\kappa}{\lambda_n^2} \sum_{m=0}^{\infty} \frac{\left(-\mu^2 T^\kappa\right)^m}{m!} E^{(m)}_{\gamma,1+\kappa+(\kappa-\gamma)m}\left(-\lambda_n^2 T^\gamma\right) \tag{4.29}$$

and

$$B_0(T) = T^\gamma E_{\kappa,1+\gamma}\left(-\mu^2 T^\kappa\right) - T^\kappa E_{\kappa,1+\kappa}\left(-\mu^2 T^\kappa\right). \tag{4.30}$$

4.3. Simplifications. In this section we show results in special cases where the solution simplifies: (i) the case of equal fractional exponents and (ii) the case of no zero eigenvalue. The first of these special cases has a clear physical interpretation. The anomalous diffusion scaling is the same along the axial direction of the cable (characterized by γ) and across the membrane (characterized by κ). In nonzero steady state conditions these two exponents should be equal. The more general case with γ and κ not equal could apply to transient states or to a zero steady state. The second special case does not have an obvious physical interpretation, but we discuss it here because it leads to a simpler mathematical solution.

4.3.1. Equal fractional exponents $\gamma = \kappa$. In this subsection we show that the solutions obtained more generally for the case $\gamma \neq \kappa$ given in sections 4.1 and 4.2 (by (4.7) and (4.23)) simplify to those given in section 2 (by (2.10)) by taking the limit $\gamma \to \kappa$ of the results in the case $\gamma \neq \kappa$.

Model I. From (4.11) with $\gamma = \kappa$,

$$A_n(T) = \mathrm{e}^{-\left(\lambda_n^2+\mu^2\right)T^\gamma}. \tag{4.31}$$

We note, from (3.8), that when $\theta = 1$,

$$\widehat{P}_\theta(s) = \frac{1}{s-\mu^2} = \frac{1}{\lambda(s)^2-\mu^2}, \tag{4.32}$$

and so from (4.6) we have $\widehat{B}_n^*(s) = 0$ and hence $B_n(T) = 0$.

Model II. From (4.25) with $\gamma = \kappa$,

$$A_n(T) = E_{\gamma,1}\left(-\left(\lambda_n^2+\mu^2\right)T^\gamma\right), \tag{4.33}$$

and from (4.21) we again find $\widehat{B}_n(s) = 0$ and hence $B_n(T) = 0$.

The potential in the case of equal exponents thus simplifies to

$$V(X,T) = \psi(X;\mu) + \sum_{n=0}^{\infty} c_n A_n(T)\Psi_n(X), \tag{4.34}$$

where $A_n(T)$ is given above for Model I and Model II. Note that when $\gamma = \kappa = 1$ both model solutions reduce to the standard solution

$$V(X,T) = \sum_{n=0}^{\infty} c_n \Psi_n(X)\exp\left(-\left(\lambda_n^2+\mu^2\right)T\right) + \psi(X;\mu). \tag{4.35}$$

4.3.2. No zero eigenvalue. We note if the system (2.12) along with the conditions (2.9) does not have a zero eigenvalue ($n \geq 1$), then it follows from (4.1) (with $\lambda = 0$) that the solution can be rewritten as

$$V(X,T) = \psi(X;0) + \sum_{n=1}^{\infty}\left[c_n^* A_n(T) + d_n B_n^{\#}(T)\right]\Psi_n(X), \tag{4.36}$$

where

$$B_n^{\#}(T) = B_n(T) + \left(\frac{1}{\lambda_n^2} - \frac{1}{\lambda_n^2+\mu^2}\right)\left(A_n(T)-1\right). \tag{4.37}$$

The Fourier coefficients, c_n^*, are then defined through

$$V(X,0) = \sum_{n=1}^{\infty} c_n^*\Psi_n(X) + \psi(X;0), \tag{4.38}$$

where

$$\psi(X;0) = \lim_{\mu\to 0}\psi(X;\mu). \tag{4.39}$$

In the case of Model I we have the explicit expression

$$B_n^{\#}(T) = -\frac{\mathrm{e}^{-\mu^2T^\kappa}}{\lambda_n^2}\sum_{m=1}^{\infty}\frac{\left(\mu^2T^\kappa\right)^m}{m!}\Gamma\left(1+\frac{\kappa}{\gamma}m\right)E_{1,1+\frac{\kappa}{\gamma}m}\left(-\lambda_n^2T^\gamma\right), \tag{4.40}$$

and in the case of Model II

$$B_n^{\#}(T) = -\frac{\mu^2T^\kappa}{\lambda_n^2}\sum_{m=0}^{\infty}\frac{\left(-\mu^2T^\kappa\right)^m}{m!}E^{(m)}_{\gamma,1+\kappa+(\kappa-\gamma)m}\left(-\lambda_n^2T^\gamma\right). \tag{4.41}$$

5. Model examples. In this section we provide details of solutions for specific combinations of the boundary conditions in (1.19). The solutions are plotted for particular values of the parameters in Figures 5.1–5.4. In the following the potential is expressed in terms of $A_n(T)$ and $B_n^{\#}(T)$, which are given by (4.11) and (4.40) for Model I and (4.25) and (4.41) for Model II.

Case 1: $a_o = a_L = 0$. When the potential is fixed at both ends of the domain there is no zero eigenvalue, and

$$V(X,T) = V_o + \frac{V_L - V_o}{L}X + \sum_{n=1}^{\infty}\left[c_n^* A_n(T) + d_n B_n^{\#}(T)\right]\sin\lambda_n X, \tag{5.1}$$

where

$$d_n = \frac{2}{L}\lambda_n\left[V_o - (-1)^n V_L\right], \quad \lambda_n = \frac{n\pi}{L}, \quad V_o = \frac{g_o}{b_o}, \quad \text{and} \quad V_L = \frac{g_L}{b_L}. \tag{5.2}$$

Representative results with $V_o = 2$, $V_L = 1$, and $\mu = 1$ are shown in Figure 5.1 for both models and for various combinations of γ, the exponent characterizing anomalous diffusion along the cable, and κ, the exponent characterizing anomalous diffusion across the membrane.

Case 2: $b_o = b_L = 0$. In the case where the derivative of the potential is fixed at both ends of the domain the limit in (4.39) does not exist, and so we cannot use (4.1) to rewrite $\psi(X;\mu)$. However, if we choose

$$\psi_o(X) = \frac{g_L}{a_L}\frac{X^2}{2L} - \frac{g_o}{a_o}\frac{(L-X)^2}{2L}, \tag{5.3}$$

then we can write

$$\psi_o(X) - \psi(X;\mu) = \left(\frac{L^2}{6} - \frac{1}{\mu^2}\right)d_o X_o(X) + \sum_{n=1}^{\infty} d_n\left(\frac{1}{\lambda_n^2} - \frac{1}{\mu^2+\lambda_n^2}\right)X_n(X), \tag{5.4}$$

where $X_n(X) = \cos\lambda_n X$ and

$$d_o = \frac{1}{L}\left[V_L^{'} - V_o^{'}\right],\ d_n = \frac{2}{L}\left[(-1)^n V_L^{'} - V_o^{'}\right],\ \lambda_n = \frac{n\pi}{L},\ V_o^{'} = \frac{g_o}{a_o},\ V_L^{'} = \frac{g_L}{a_L}. \tag{5.5}$$

The potential can then be written as

$$V(X,T) = \frac{V_L^{'}X^2 - V_o^{'}(L-X)^2}{2L} + \sum_{n=0}^{\infty}\left[c_n^* A_n(T) + d_n B_n^{\#}(T)\right]\cos\lambda_n X, \tag{5.6}$$

where, in addition to (4.37), we have

$$B_0^{\#}(T) = B_0(T) + \left(\frac{L^2}{6} - \frac{1}{\mu^2}\right)\left(A_0(T) - 1\right). \tag{5.7}$$

In the case of Model I this simplifies to

$$B_0^{\#}(T) = -\left(1 - A_0(T)\right)\frac{L^2}{6} + T^{\gamma}\Gamma\left(1+\frac{\gamma}{\kappa}\right)E_{1,1+\frac{\gamma}{\kappa}}\left(-\mu^2 T^{\kappa}\right), \tag{5.8}$$

and for Model II

$$B_0^{\#}(T) = -\left(1 - A_0(T)\right)\frac{L^2}{6} + T^{\gamma}E_{\kappa,1+\gamma}\left(-\mu^2 T^{\kappa}\right). \tag{5.9}$$

In (5.6) the constants c_n^* are now defined through the initial conditions

$$V(X,0) = \psi_o(X) + \sum_{n=0}^{\infty} c_n^* \cos\lambda_n X. \tag{5.10}$$

Results in the case of $V_o^{'} = -2$, $V_L^{'} = -1$, and $\mu = 1$ are shown for both models in Figure 5.2.

Case 3: $a_o = b_L = 0$. The solution with a fixed potential at $X = 0$ and a fixed derivative at $X = L$ is given by

$$V(X,T) = V_o + V_L^{'}X + \sum_{n=1}^{\infty}\left[c_n^* A_n(T) + d_n B_n^{\#}(T)\right]\sin\lambda_n X, \tag{5.11}$$

where

$$d_n = \frac{2}{L}\left[\lambda_n V_o - (-1)^n V_L^{'}\right], \quad \lambda_n = \frac{(2n-1)\pi}{2L}, \quad V_o = \frac{g_o}{b_o}, \quad \text{and} \quad V_L^{'} = \frac{g_L}{a_L}. \tag{5.12}$$

Figure 5.3 shows the effect of the fractional exponents on the solution of both models in the case of $V_o = 2$, $V_L^{'} = -1$, and $\mu = 1$.

Case 4: $a_L = b_o = 0$. For this case we consider the reverse of Case 3 with a fixed potential at $x = L$ and a fixed derivative at $x = 0$. The solution is given by

$$V(X,T) = V_L - V_o^{'}(L - X) + \sum_{n=1}^{\infty}\left[c_n^* A_n(T) + d_n B_n^{\#}(T)\right]\cos\lambda_n X, \tag{5.13}$$

where

$$d_n = -\frac{2}{L}\left[(-1)^n\lambda_n V_L + V_o^{'}\right], \quad \lambda_n = \frac{(2n-1)\pi}{2L}, \quad V_L = \frac{g_L}{b_L}, \quad \text{and} \quad V_o^{'} = \frac{g_o}{a_o}. \tag{5.14}$$

Solutions with the parameters $V_o^{'} = 2$, $V_L = -1$, and $\mu = 1$ are shown in Figure 5.4 for each model given various combinations of γ and κ.

5.1. Plots of solutions. Here we display plots of solutions of the fractional cable equations (1.17) and (1.18) for a finite cable of dimensionless length $L = 1$ and the following boundary conditions: (i) voltage clamped at both ends of the cable, $V(X,0) = 2$ and $V(X,1) = 1$ (Figure 5.1); (ii) standard current injection (nonzero potential gradients) at both ends of the cable, $V_X(X,0) = -2$ and $V_X(X,1) = -1$ (Figure 5.2); (iii) voltage clamped at the left end of the cable and standard current injection at the right end, $V(X,0) = 2$ and $V_X(X,1) = -1$ (Figure 5.3); and (iv) standard current injection at the left end of the cable and voltage clamped at the right end of the cable, $V_X(X,0) = -1$ and $V(X,1) = 1$ (Figure 5.4). Solutions are shown at the dimensionless times $T = 0.1$, 1.0, 10.0, and 100.0 with the constant $\mu = 1$ and the anomalous exponents (a) $\gamma = \kappa = 1$, (b) $\gamma = \kappa = 1/2$, (c) $\gamma = 1/2$ and $\kappa = 1$, and (d) $\gamma = 1$ and $\kappa = 1/2$. These values for the anomalous exponents have been selected

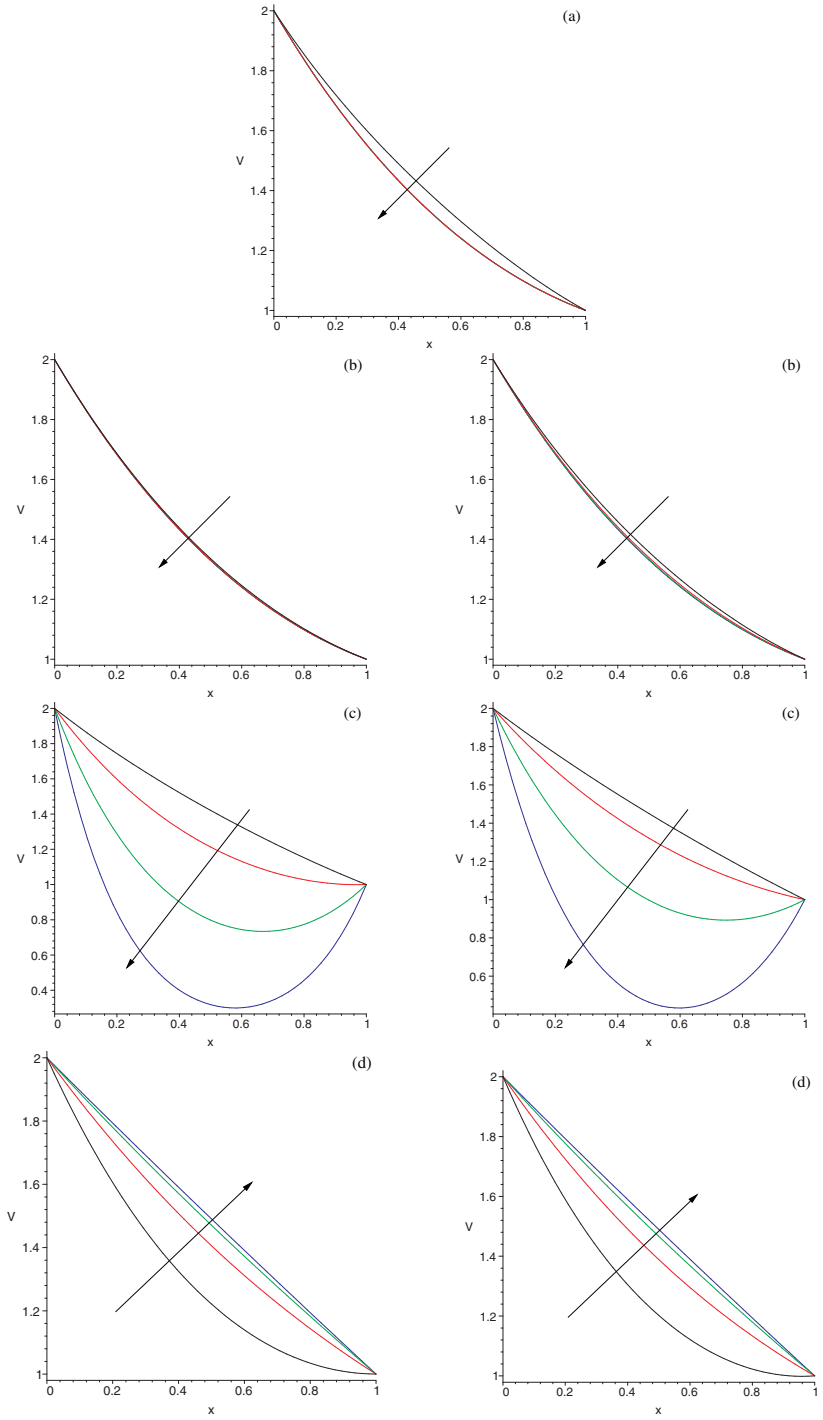

FIG. 5.1. *Fractional cable equation solutions (Model* I*, left, and Model* II*, right) in a finite cable for* (a) *the standard cable equation,* $\gamma = \kappa = 1$, (b) $\gamma = \kappa = 1/2$, (c) $\gamma = 1/2$ *and* $\kappa = 1$, *and* (d) $\gamma = 1$ *and* $\kappa = 1/2$ *at* $T = 0.1$, 1, 10, *and* 100 *with boundary conditions* $V(0,T) = 2$ *and* $V(1,T) = 1$. *Time increases in the direction of the arrow.*

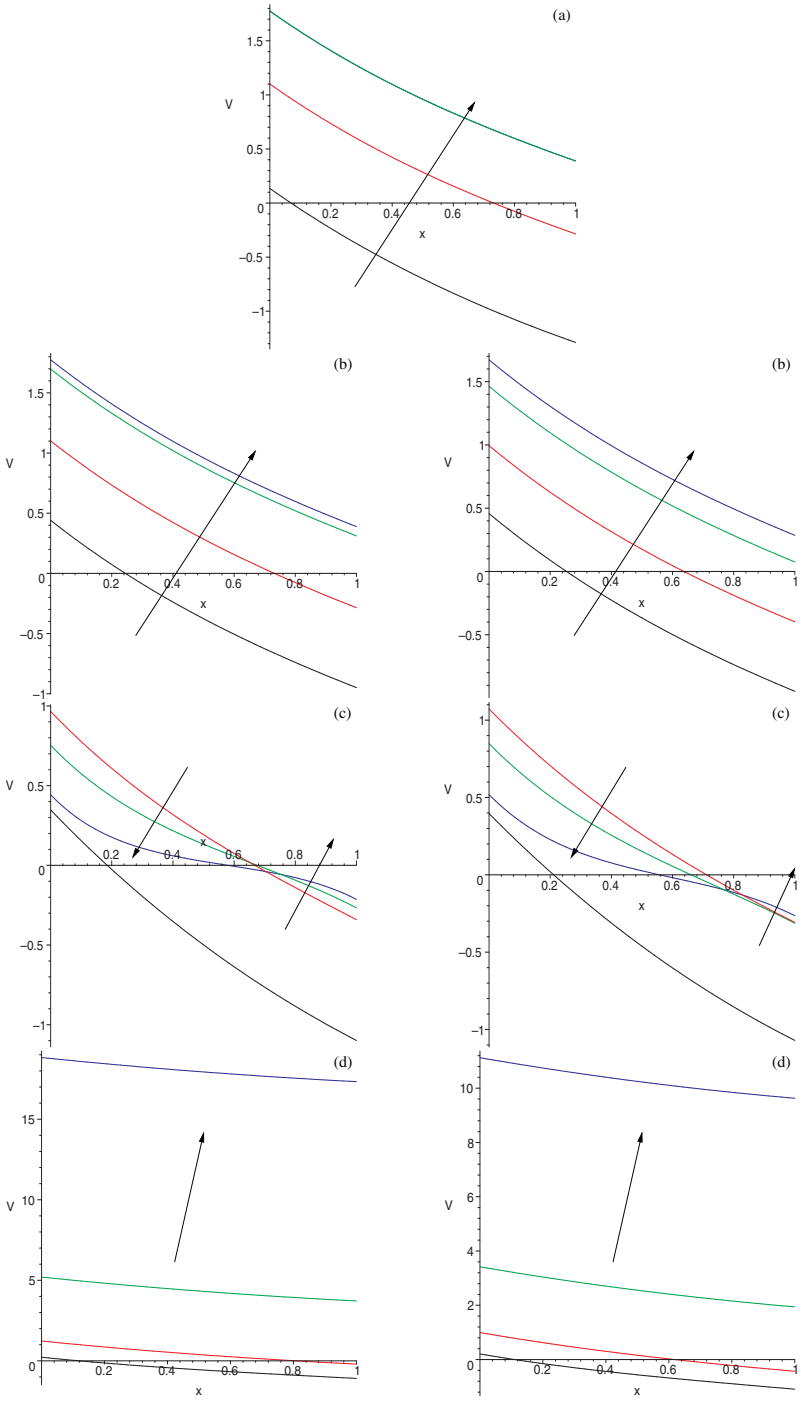

FIG. 5.2. *Fractional cable equation solutions (Model* I*, left, and Model* II*, right) in a finite cable for* (a) *the standard cable equation,* $\gamma = \kappa = 1$, (b) $\gamma = \kappa = 1/2$, (c) $\gamma = 1/2$ *and* $\kappa = 1$, *and* (d) $\gamma = 1$ *and* $\kappa = 1/2$ *at* $T = 0.1$, 1, 10, *and* 100 *with boundary conditions* $V_X(0,T) = -2$ *and* $V_X(1,T) = -1$. *Time increases in the direction of the arrow except in* (c) *(see text).*

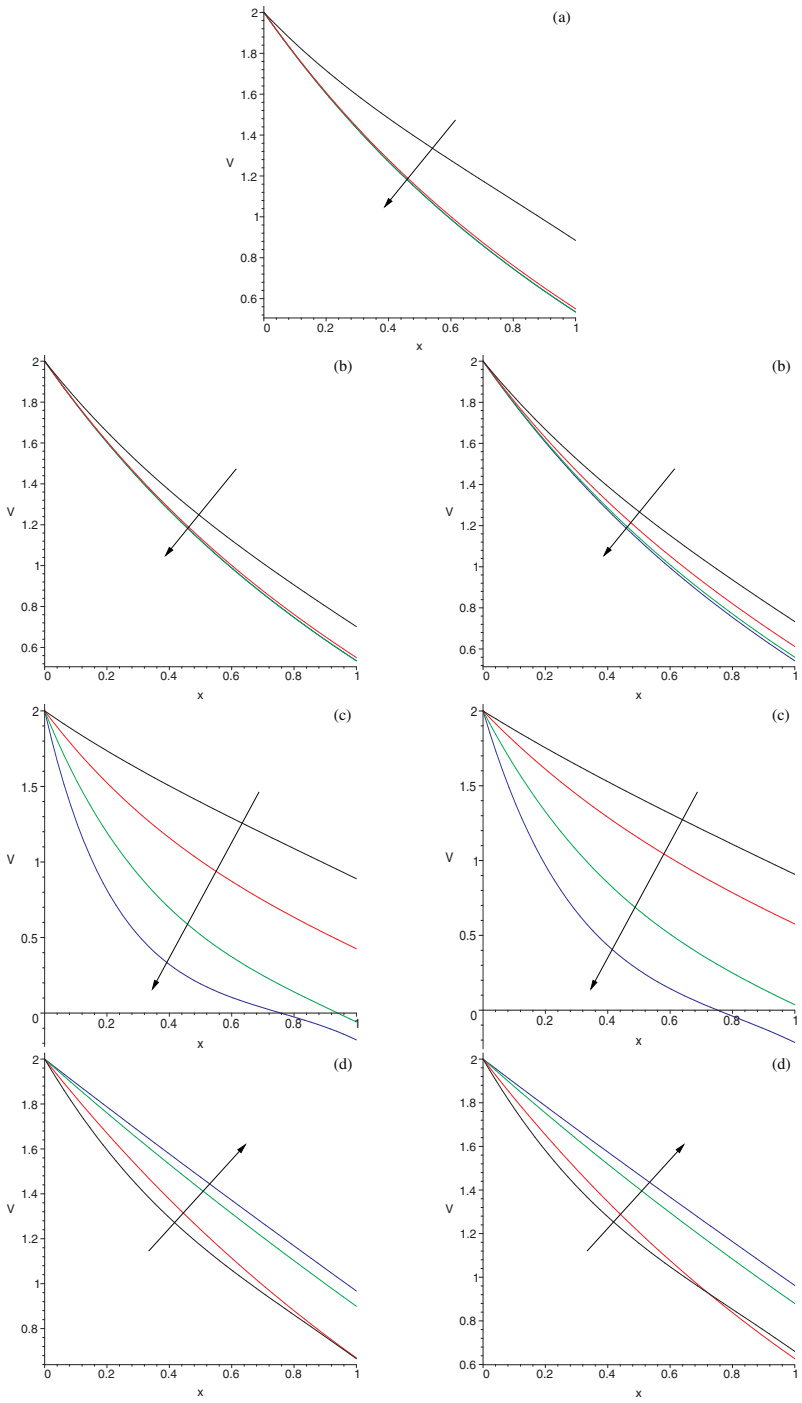

FIG. 5.3. *Fractional cable equation solutions (Model* I*, left, and Model* II*, right) in a finite cable for* (a) *the standard cable equation,* $\gamma = \kappa = 1$, (b) $\gamma = \kappa = 1/2$, (c) $\gamma = 1/2$ *and* $\kappa = 1$, *and* (d) $\gamma = 1$ *and* $\kappa = 1/2$ *at* $T = 0.1$, 1, 10, *and* 100 *with boundary conditions* $V(0,T) = 2$ *and* $V_X(1,T) = -1$. *Time increases in the direction of the arrow.*

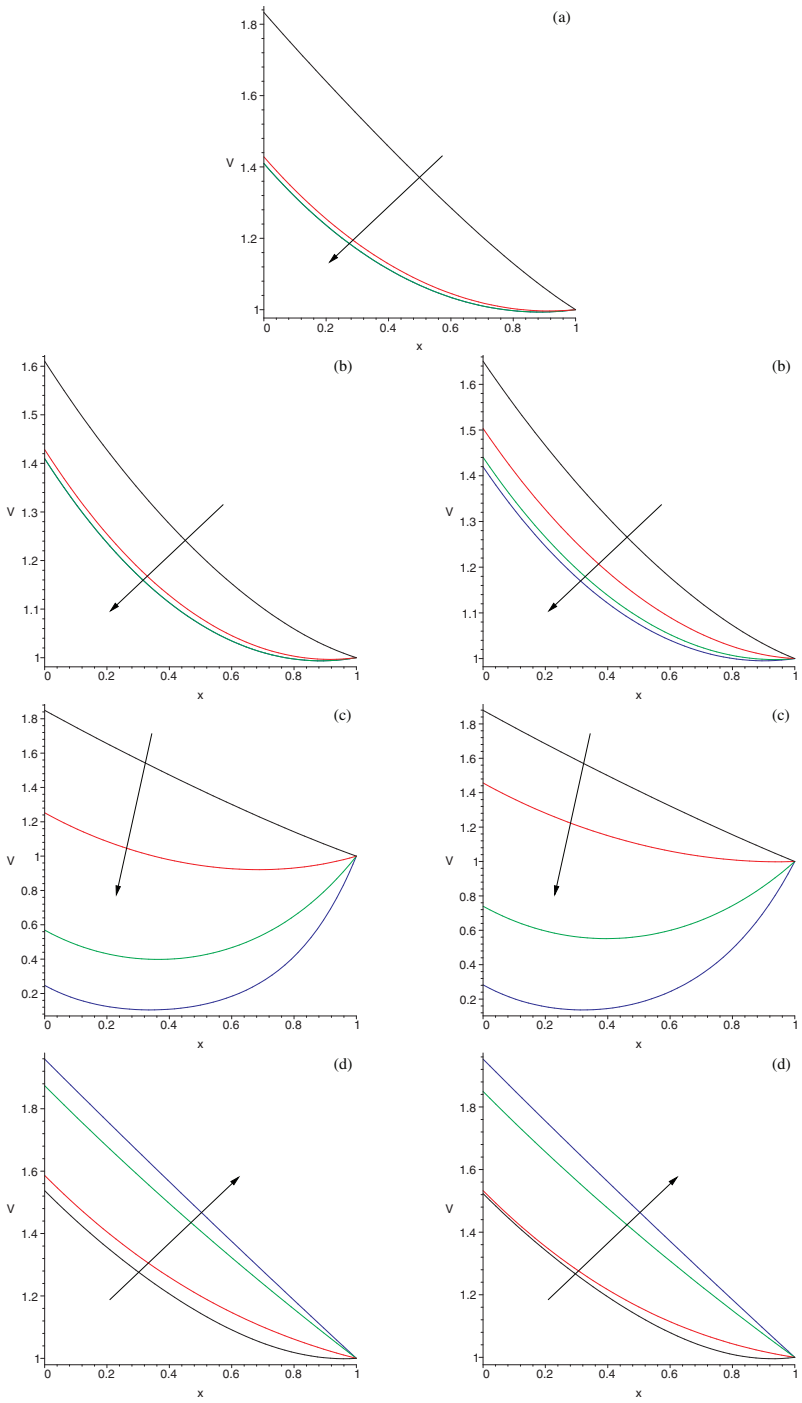

FIG. 5.4. *Fractional cable equation solutions (Model* I*, left, and Model* II*, right) in a finite cable for* (a) *the standard cable equation,* $\gamma = \kappa = 1$, (b) $\gamma = \kappa = 1/2$, (c) $\gamma = 1/2$ *and* $\kappa = 1$, *and* (d) $\gamma = 1$ *and* $\kappa = 1/2$ *at* $T = 0.1$, 1, 10, *and* 100 *with boundary conditions* $V_X(0,T) = -1$ *and* $V(1,T) = 1$. *Time increases in the direction of the arrow.*

to exhibit the range of behaviors that can occur. The case $\gamma = \kappa = 1$ corresponds to the standard cable equation for the given boundary conditions.

In Figures 5.1, 5.3, and 5.4 the initial condition was taken as the linear function $V(X,0) = 2 - X = \psi(X;0)$. This choice satisfies the boundary conditions and sets the constants c_n^* to zero. In the mixed boundary example, Case 2, shown in Figure 5.2, we have used instead the initial condition $V(X,0) = -2X + X^2/2$.

In general the direction of the arrows indicates the chronological order of the solution except in part (c) of Figure 5.2, where the solution at $T = 0.1$ is given by the lowest curve and is then followed by the remaining curves in the order indicated by the arrow. Note that, in the particular case (a) of standard diffusion in each figure, the solution at $T = 100$ is practically indistinguishable from the result at $T = 10$, as by this time, the plots indicate that a steady state has effectively been reached.

A comparison of the results for both models, given the same boundary conditions and the same anomalous exponents, shows the same qualitative behavior (compare the left and right sides of the figures). The main difference between the models is the speed of temporal evolution; the results for Model I evolve slightly faster than those for Model II. From Appendix E we see that for both long and short times the behaviors of the functions $A_n(T)$, $B_n(T)$, and $B_n^{\#}(T)$ of both models comprising the solution are asymptotically similar. The differences arise from the magnitude of the coefficients of the correction terms.

In the cases where the fractional exponents are equal ((a) and (b)) the solution converges to the appropriate hyperbolic steady state $V(X,0) = \psi(X;\mu)$, which satisfies the boundary conditions. Here when $\gamma = \kappa = 1/2$, the solution takes longer to reach the steady state due to anomalous diffusion, as expected. However, if the exponents are not equal, as in Cases (c) and (d), the hyperbolic steady state is not reached.

In Case (c), where the subdiffusion is more anomalous along the nerve cell than across the nerve cell ($\gamma < \kappa$), the behavior of the solutions is quite different from that of the equal exponent cases ((a) and (b)). We see in part (c) of Figures 5.1–5.4 that the solution decays toward zero, as predicted in Appendix E in (E.37). The solution also has regions of negative potential for both models in Figure 5.3 at the end of the cable. This phenomenon is due to the presence of boundary layers at the ends of the domain.

In Case (d), where the subdiffusion is more anomalous across the nerve cell than along the nerve cell ($\gamma > \kappa$), we see in Figures 5.1, 5.3, and 5.4 that the solution appears to converge back to, in our case, the initial condition $V(X,0) = \psi(X;0)$ after initially moving away from it. This counterintuitive result can be explained by the behavior of the cable equations at long times. For Model I, with $\gamma = 1$ and $\kappa = \frac{1}{2}$, the effect of the last term of (1.17) will decay to zero if V remains constant. As such, the cable equation will act like the diffusion equation, which has linear steady state given the boundary conditions imposed in these figures. The same explanation can be applied to the result of Model II. If the potential remains constant in time for sufficiently long times, then the fractional derivative of the last term in (1.18) acts like that of Model I. That is, the Riemann fractional derivative of a constant is

$$\frac{\partial^{1-\kappa}}{\partial T^{1-\kappa}} c = \frac{cT^{\kappa-1}}{\Gamma(\kappa)}. \tag{5.15}$$

Even though the potential is not constant for all times (especially initially), this result still applies as the contribution of the initial transient variation of $V(X,T)$ diminishes

and can be ignored [24, 22]. Our analysis in Appendix E also shows that this behavior is indeed possible for all $\gamma > \kappa$ as given by (E.31). In Figure 5.2, however, this behavior is not repeated, but rather the solution for both models seems to grow with time, and no steady state is reached. The difference in these two behaviors can be explained by the presence of $B_o^{\#}(T)$ in the solution for the potential which is not included for the other boundary condition examples. The function $B_o^{\#}(T)$, in the case of both models, is shown in Appendix E to grow like $T^{\gamma-\kappa} = \sqrt{T}$ in Case (d) as seen in (E.32) and hence leads to growing solutions.

5.2. Justification of the long time asymptotic results. The long time behaviors obtained in Case (c) ($\gamma < \kappa$) and Case (d) ($\gamma > \kappa$) can be explained by rescaling time as $U = T^{\kappa}$ and $U = T^{\gamma}$, respectively.

The governing model equations for Case (c) with $U = T^{\kappa}$ and $W = V(X, T^{\kappa})$ are as follows:

$$\text{Model I} \qquad \frac{\partial W}{\partial U} = \frac{\gamma}{\kappa} U^{\frac{\gamma}{\kappa}-1} \frac{\partial^2 W}{\partial X^2} - \mu^2 W$$

and

$$\text{Model II} \qquad \frac{\partial W}{\partial U} = \frac{1}{\kappa} U^{\frac{\gamma}{\kappa}-1} \left(P^{\gamma,1-\gamma}_{-\frac{1}{\kappa}} \frac{\partial^2 W}{\partial X^2} \right)(U) - \frac{\mu^2}{\kappa} \left(P^{\kappa,1-\kappa}_{-\frac{1}{\kappa}} W \right)(U),$$

where $(P^{\tau,\alpha}_{\beta} r)(z)$ is an Erdelyi–Kober fractional differential operator [6]. In both models, since $\gamma < \kappa$ the coefficient of the first term on the left goes to zero for large U, and the model equations behave as fractional decay equations with zero steady states, provided that the boundary conditions can be satisfied. The "loss" of the spatial derivative in this regime means that the boundary conditions are not satisfied exactly and boundary layers form. This is precisely the behavior that we found in the asymptotic analysis of the general solutions, (E.37), and the behavior that we observed in the figures.

The governing model equations for Case (d) with $U = T^{\gamma}$ and $W = V(X, T^{\gamma})$ are as follows:

$$\text{Model I} \qquad \frac{\partial W}{\partial U} = \frac{\partial^2 W}{\partial X^2} - \mu^2 \frac{\kappa}{\gamma} U^{\frac{\kappa}{\gamma}-1} W$$

and

$$\text{Model II} \qquad \frac{\partial W}{\partial U} = \frac{1}{\gamma} \left(P^{\gamma,1-\gamma}_{-\frac{1}{\gamma}} \frac{\partial^2 W}{\partial x^2} \right)(U) - \frac{\mu^2}{\gamma} U^{\frac{\kappa}{\gamma}-1} \left(P^{\kappa,1-\kappa}_{-\frac{1}{\gamma}} W \right)(U).$$

In both models, since $\kappa < \gamma$ the coefficient of the second term on the left goes to zero for large U, and the model equations behave as fractional diffusion equations with the spatially linear steady state, provided that the boundary conditions can be satisfied. This is the behavior that we found in the asymptotic analysis of the general solutions, (E.31), and the behavior that we observed in the figures.

6. Conclusions. In this paper we investigated the behavior of the finite domain solutions for fractional cable equations, originally introduced to model passive potential propagation in spiny dendrites in [14]. We derived the solutions for two models of the anomalous diffusion, (1.17) and (1.18), with general mixed Robin boundary conditions applied at the ends of the cable. Solutions in the infinite and semi-infinite domains were reported in an earlier paper [17].

The qualitative behavior of the solutions was found to be similar in both models, given similar scaling exponents and boundary conditions. However, model-dependent differences were manifest in the rates of temporal evolution of the solutions. The model solutions were found to be strongly impacted by the anomalous subdiffusion scaling exponents $0 < \gamma \leq 1$ and $0 < \kappa \leq 1$. These exponents quantify the anomalous subdiffusion along the axial direction of a nerve cell (γ) and across a nerve cell membrane (κ). The subdiffusion is more anomalous for lower values of the exponents, and standard cable equation results are recovered for $\gamma = \kappa = 1$. The most significant departures from standard cable results were obtained when the values of these exponents were different. If these exponents were equal, but fractional, then the standard hyperbolic steady state was approached in the long time limit, but the rate of approach was slowed by the anomalous diffusion. If the subdiffusion was more anomalous along the axial direction than across the membrane ($\gamma < \kappa$), then the solution decayed toward zero in the long time limit, but with boundary layers arising from the imposed boundary conditions. If the subdiffusion was more anomalous across the cell membrane ($\gamma > \kappa$), the solution approached a spatially linear steady state after long times. This behavior, though at first counterintuitive, is consistent with diffusion equation behavior, which can be reconciled by considering that the axial diffusion characterized by γ dominates over the transmembrane diffusion characterized by κ, and it is the latter that contributes to drift in the electric field.

The results in this paper are a starting point for using fractional cable equations to model passive potential propagation in spiny nerve cells and other nerve cells with anomalous subdiffusion, but the results are contingent on experimental calibration of the two models. Remarkably, both models exhibit very similar behaviors across the range of behaviors found for different boundary conditions and different exponents. On the other hand, unless the two anomalous scaling exponents are equal, the behaviors are very different from those predicted by the standard cable theory. This is a clear demonstration that anomalous diffusion can strongly impact cable properties and the way that it impacts is not particularly sensitive to model-dependent peculiarities in the implementation of the anomalous diffusion.

In applications to whole nerve cell signaling further consideration will be required for physically relevant boundary conditions including time-dependent currents (fractional or otherwise) at the end of branch segments. We plan to explore these issues in future work.

Appendix A. Evaluation of fractional integral for initial value problems. We note that in solving the fractional cable equation, (1.18), we specify only the initial value of the potential, $V(x, 0)$, in addition to the boundary conditions. But note, as in section 3.2, that when we take the Laplace transform of (1.18), we find fractional integral terms of the form

$$\left[\frac{\partial^{-\beta}}{\partial t^{-\beta}} V(x,t)\right|_{t=0} \tag{A.1}$$

with $0 < \beta \leq 1$ due to the presence of the Riemann–Liouville fractional derivatives. We show here that these terms are zero.

We apply the initial value theorem for Laplace transforms

$$\lim_{s\to\infty} s\widehat{f}(s) = \lim_{t\to 0^+} f(t) = f(0) \tag{A.2}$$

to the potential, $V(x,t)$,

$$\lim_{s\to\infty} s\widehat{V}(x,s) = \lim_{t\to 0} V(x,t) = V(x,0), \tag{A.3}$$

which implies that for large s

$$\widehat{V}(x,s) \sim \frac{V(x,0)}{s} + O\left(\frac{1}{s^{1+\alpha}}\right) \tag{A.4}$$

for some $\alpha > 0$. Now to evaluate the value of the fractional integral at $t = 0$ we note that [24]

$$\mathcal{L}\left\{\frac{\partial^{-\beta}}{\partial t^{-\beta}} V(x,t)\right\}(s) = s^{-\beta}\widehat{V}(x,s), \tag{A.5}$$

and so using (A.4) we find

$$\mathcal{L}\left\{\frac{\partial^{-\beta}}{\partial t^{-\beta}} V(x,t)\right\}(s) \sim \frac{V(x,0)}{s^{1+\beta}} + O\left(\frac{1}{s^{1+\alpha+\beta}}\right). \tag{A.6}$$

Again applying the initial value theorem (A.2) we find

$$\lim_{t\to 0} \frac{\partial^{-\beta}}{\partial t^{-\beta}} V(x,t) = \lim_{s\to\infty} s\mathcal{L}\left\{\frac{\partial^{-\beta}}{\partial t^{-\beta}} V(x,t)\right\}(s) = \lim_{s\to\infty} \frac{V(x,0)}{s^{\beta}} + O\left(\frac{1}{s^{\alpha+\beta}}\right) = 0. \tag{A.7}$$

That is, for the initial value problem of (1.18), the fractional integrals are indeed zero. The same result follows for the fractional integral of $\frac{\partial^2 V}{\partial x^2}$ by interchanging the order of temporal and spatial differentiation.

Appendix B. The Mittag–Leffler function. Here we introduce and list some useful identities involving the Mittag–Leffler function and its derivative. The kth derivative of the Mittag–Leffler function is

$$E^{(k)}_{\alpha,\beta}(y) = \frac{d^k E_{\alpha,\beta}(y)}{dy^k} = \sum_{j=0}^{\infty} \frac{(j+k)!\, y^j}{j!\, \Gamma(\alpha(j+k)+\beta)}, \tag{B.1}$$

and its Laplace transform is given by

$$\mathcal{L}\left\{t^{\alpha k+\beta-1} E^{(k)}_{\alpha,\beta}(-at^{\alpha})\right\}(s) = \frac{k!\, s^{\alpha-\beta}}{(s^{\alpha}+a)^{k+1}}. \tag{B.2}$$

Full details and properties can be found in [24].

We have the following identity for the Mittag–Leffler function for $z \neq 0$:

$$E_{\alpha,\alpha+\beta}(z) = \frac{1}{z}\left(E_{\alpha,\beta}(z) - \frac{1}{\Gamma(\beta)}\right), \tag{B.3}$$

and

$$E_{\alpha,\alpha+\beta}(z) = \frac{1}{\Gamma(\alpha+\beta)} \tag{B.4}$$

when $z = 0$. The last equation follows from the definition of the Mittag–Leffler function with $k = 0$ in (B.1).

Particular cases of the Mittag–Leffler function are the confluent hypergeometric function

$$\Gamma(\beta)\, E_{1,\beta}(z) = {}_1F_1(1;\beta;z) \tag{B.5}$$

and the exponential function

$$E_{1,1}(z) = \mathrm{e}^z. \tag{B.6}$$

For large values of the argument z we have the asymptotic behavior for the Mittag–Leffler function [41, 23],

$$E_{\alpha,\beta}(z) \sim -\sum_{n=1}^{N-1} \frac{z^{-n}}{\Gamma(\beta-\alpha n)} + O(z^{-N}) \ \text{ as } \ z \to -\infty, \tag{B.7}$$

and for its kth derivative

$$E^{(k)}_{\alpha,\beta}(z) \sim (-z)^{-(1+k)} \sum_{\nu=0}^{\infty} \frac{z^{-\nu}\,(k+\nu)!}{\nu!\,\Gamma(\beta-\alpha(1+\nu))} \ \text{ as } \ z \to -\infty. \tag{B.8}$$

The latter result can be found from rewriting the derivative of the Mittag–Leffler function as a Fox function [19, 16] and then using the asymptotic approximation for Fox functions [4].

Appendix C. Solution of a second order differential equation. For both models (1.17) and (1.18) we need to solve a second order differential equation of the form

$$\frac{\partial^2 \widehat{y}}{\partial x^2} - \lambda^2(s)\widehat{y} = -\alpha(s)V(x,0) \tag{C.1}$$

along with the boundary conditions

$$a_o \frac{\partial \widehat{y}(0,s)}{\partial x} + b_o \widehat{y}(0,s) = g_o\beta(s) \quad \text{and} \quad a_L \frac{\partial \widehat{y}(L,s)}{\partial x} + b_L \widehat{y}(L,s) = g_L\beta(s), \tag{C.2}$$

where for Model I, $\alpha(s) = 1$ and $\beta(s) = \widehat{P}_\theta(s)$, and for Model II, $\alpha(s) = s^{\gamma-1}$ and $\beta(s) = 1/s$.

Solving (C.1) we find

$$\begin{aligned} \widehat{y}(x,s) = {} & c_1 \cosh\lambda(s)x + c_2 \sinh\lambda(s)x \\ & - \frac{\alpha(s)}{\lambda(s)} \int_0^x \sinh\left[\lambda(s)\,(x-x')\right] V(x',0)\, dx', \end{aligned} \tag{C.3}$$

where the constants, c_1 and c_2, may be functions of the Laplace variable, s. Now using (2.3) we can now evaluate the integral in (C.3). Noting that $\psi(x;\mu)$ satisfies (2.5) it can be shown that

$$\begin{aligned} \int_0^x \sinh\left[\lambda(s)\,(x-x')\right] \psi(x';\mu)\, dx' = {} & \frac{\lambda(s)}{\lambda^2(s)-\mu^2} \left(\psi(0;\mu)\cosh\lambda(s)x - \psi(x;\mu)\right) \\ & + \frac{1}{\lambda^2-\mu^2}\psi'(0;\mu)\sinh\lambda(s)x, \end{aligned} \tag{C.4}$$

and likewise, with $\Psi_n(x)$ satisfying (2.12), we have

$$\int_0^x \sinh\left[\lambda(s)\left(x-x'\right)\right]\Psi_n(x')\,dx' = \frac{\lambda}{\lambda^2(s)+\lambda_n^2}\left(\Psi_n\left(0\right)\cosh\lambda(s)x - \Psi_n\left(x\right)\right) \tag{C.5}$$

$$+\frac{1}{\lambda^2(s)+\lambda_n^2}\Psi_n^{'}\left(0\right)\sinh\lambda(s)x. \tag{C.6}$$

The solution of (C.1) can then be expressed as

$$\widehat{y}(x,s) = d_1\cosh\lambda(s)x + d_2\sinh\lambda(s)x + \frac{\alpha(s)}{\lambda^2(s)-\mu^2}\psi(x;\mu) + \sum_{n=0}^{\infty}\frac{\alpha(s)}{\lambda^2(s)+\lambda_n^2}c_n\Psi_n(x), \tag{C.7}$$

where we have absorbed the constant coefficients appearing in (C.4) and (C.6), as well as the constants c_1 and c_2, into d_1 and d_2.

Applying the boundary conditions in (C.2) and using (2.6) and (2.9) we arrive at

$$\widehat{y}(x,s) = \left(\beta(s) - \frac{\alpha(s)}{\lambda^2(s)-\mu^2}\right)\psi(x;\lambda(s)) + \frac{\alpha(s)}{\lambda^2(s)-\mu^2}\psi(x;\mu) + \sum_{n=0}^{\infty}\frac{\alpha(s)}{\lambda^2(s)+\lambda_n^2}c_n\Psi_n(x). \tag{C.8}$$

Appendix D. Inverse Laplace transforms. In this appendix we consider the inverse Laplace transform for $\widehat{B}_n^*(s)$. First note from (4.6) that we can write

$$\widehat{B}_n^*(s) = -\frac{\mu^2}{\lambda_n^2\left(\lambda_n^2+\mu^2\right)}\left(\widehat{A}_n^*(s) - \widehat{P}_\theta(s)\right) - \frac{1}{\lambda_n^2}\widehat{A}_n^*(s)\mathcal{L}\left\{\frac{dP_\theta}{d\tau}\right\}(s), \tag{D.1}$$

and then we have the inverse

$$B_n^*(\tau) = \frac{1}{\lambda_n^2+\mu^2}\left(A_n^*(\tau) - P_\theta(\tau)\right) + \int_0^\tau P_\theta(w)A_n^*(\tau-w)\,dw. \tag{D.2}$$

To evaluate the convolution integral we first expand $P_\theta(w)$ as Taylor series to give

$$\int_0^\tau P_\theta(w)A_n^*(\tau-w)\,dw = \sum_{m=0}^{\infty}\frac{\mu^{2m}}{m!}\int_0^\tau w^{\theta m}\mathrm{e}^{-\lambda_n^2(\tau-w)}\,dw. \tag{D.3}$$

Now the simpler convolution integral can be evaluated with the use of Laplace transforms,

$$\mathcal{L}\left\{\int_0^\tau w^{\theta m}\mathrm{e}^{-\lambda_n^2(\tau-w)}\,dw\right\}(s) = \Gamma\left(1+\theta m\right)\frac{s^{-(1+\theta m)}}{s+\lambda_n^2}, \tag{D.4}$$

and using (B.2) we then find

$$\int_0^\tau w^{\theta m}\mathrm{e}^{-\lambda_n^2(\tau-w)}\,dw = \Gamma\left(1+\theta m\right)\tau^{1+\theta m}E_{1,2+\theta m}\left(-\lambda_n^2\tau\right), \tag{D.5}$$

where $E_{\alpha,\beta}(z)$ is the Mittag–Leffler function given in (B.1) [24].

If $\lambda_n \neq 0$, this integral can be written, with the use of (B.3), as

$$\int_0^\tau w^{\theta m}\mathrm{e}^{-\lambda_n^2(\tau-w)}\,dw = \frac{\tau^{\theta m}}{\lambda_n^2}\left[1-\Gamma\left(1+\theta m\right)E_{1,1+\theta m}\left(-\lambda_n^2\tau\right)\right], \tag{D.6}$$

and (D.3) becomes

(D.7)
$$\int_0^\tau P_\theta(w)A_n^*(\tau-w)\,dw=\frac{1}{\lambda_n^2}\left[\mathrm{e}^{\mu^2\tau^\theta}-\sum_{m=0}^{\infty}\frac{\left(\mu^2\tau^\theta\right)^m}{m!}\Gamma\left(1+\theta m\right)E_{1,1+\theta m}\left(-\lambda_n^2\tau\right)\right].$$

In the case $\lambda_0=0$ and using (D.5), (D.3) simplifies to

$$\int_0^\tau P_\theta(w)\,dw=\frac{\tau}{\theta}\sum_{m=0}^{\infty}\frac{\left(\mu^2\tau^\theta\right)^m}{m!}\frac{\Gamma\left(m+\dfrac{1}{\theta}\right)}{\Gamma\left(m+1+\dfrac{1}{\theta}\right)}=\tau\,{}_1F_1\left(\frac{1}{\theta};1+\frac{1}{\theta};\mu^2\tau^\theta\right),\tag{D.8}$$

where ${}_1F_1(z)$ is a hypergeometric function [1].

Appendix E. Finite solution asymptotics. In this appendix we discuss the temporal behavior of the solutions of fractional cable equations (1.17) and (1.18) which can be written succinctly as

$$V(x,t)=\psi(x;\mu)+\sum_{n=0}^{\infty}\left[c_nA_n(t)+d_nB_n(t)\right]\Psi_n(x)\tag{E.1}$$

or (4.36),

$$V(x,t)=\psi(x;0)+\sum_{n=0}^{\infty}\left[c_n^*A_n(t)+d_nB_n^{\#}(t)\right]\Psi_n(x)\tag{E.2}$$

with the appropriately defined values for the constants and the functions $\psi(x;\mu)$ and $\psi(x,0)$ (or $\psi_o(x)$ when there is a zero eigenvalue).

To investigate the temporal behavior of the solutions (E.1) and (E.2) we need only consider the temporal behavior of the functions $A_n(t)$, $B_n(t)$, and $B_n^{\#}(t)$. We concentrate here on the functions $A_n(t)$ and $B_n(t)$. The temporal behavior of $B_n^{\#}(t)$ can then be obtained via (4.37) and (5.7).

E.1. Small *t*.

Model I. Using the definition of exponential and the Mittag–Leffler function in (B.1) we can express functions $A_n(t)$, $B_n(t)$, and $B_n^{\#}(t)$ as series for small t. The approximation for $A_n(t)$, in (4.11), is

$$A_n(t)\sim 1-\left(\lambda_n^2t^\gamma+\mu^2t^\kappa\right)+O\left(t^{\min(2\gamma,2\kappa,\gamma+\kappa)}\right),\tag{E.3}$$

and when $\lambda_n=0$,

$$A_o(t)\sim 1-\mu^2t^\kappa+O\left(t^{2\kappa}\right).\tag{E.4}$$

The approximations for $B_n(t)$ and $B_o(t)$, using (4.14) and (4.18), are

$$B_n(t)\sim\begin{cases}\dfrac{\mu^2t^\gamma}{\lambda_n^2+\mu^2}+O\left(t^{\min(2\gamma,\kappa)}\right), & \gamma<\kappa,\\ -\dfrac{\mu^2t^\kappa}{\lambda_n^2+\mu^2}+O\left(t^{\min(2\kappa,\gamma)}\right), & \gamma>\kappa,\\ 0, & \gamma=\kappa,\end{cases}\tag{E.5}$$

and

$$B_o(t) \sim \begin{cases} t^\gamma + O\left(t^\kappa\right), & \gamma < \kappa, \\ -t^\kappa + O\left(t^{\min(2\kappa,\gamma)}\right), & \gamma > \kappa, \\ 0, & \gamma = \kappa. \end{cases} \tag{E.6}$$

Now using the respective equations (4.37) and (5.7), we find the short-time behaviors

$$B_n^{\#}(t) \sim -\frac{\mu^2 t^\kappa}{\lambda_n^2} + O\left(t^{\min(2\kappa,\gamma+\kappa)}\right), \tag{E.7}$$

$$B_o^{\#}(t) \sim -\frac{\mu^2 L^2 t^\kappa}{6} + t^\gamma + O\left(t^{\min(2\kappa,\gamma+\kappa)}\right). \tag{E.8}$$

Model II. Again using the definition of the derivative of the Mittag–Leffler function in (B.1) we can express functions $A_n(t)$, $B_n(t)$, and $B_n^{\#}(t)$ as series for small t. The approximation for $A_n(t)$, given in (4.25), is

$$A_n(t) \sim 1 - \left(\frac{\lambda_n^2 t^\gamma}{\Gamma(1+\gamma)} + \frac{\mu^2 t^\kappa}{\Gamma(1+\kappa)}\right) + O\left(t^{\min(2\gamma,2\kappa,\gamma+\kappa)}\right) \tag{E.9}$$

and when $\lambda_n = 0$,

$$A_o(t) \sim 1 - \frac{\mu^2 t^\kappa}{\Gamma(1+\kappa)} + O\left(t^{2\kappa}\right), \tag{E.10}$$

which shows that $A_n(0) = 1$ for all n.

The small time behaviors of the functions $B_n(t)$ and $B_o(t)$ using (4.29) and (4.30) are given by

$$B_n(t) \sim \begin{cases} \dfrac{\mu^2 t^\gamma}{(\lambda_n^2+\mu^2)\Gamma(1+\gamma)} + O\left(t^{\min(2\gamma,\kappa)}\right), & \gamma < \kappa, \\ -\dfrac{\mu^2 t^\kappa}{(\lambda_n^2+\mu^2)\Gamma(1+\kappa)} + O\left(t^{\min(2\kappa,\gamma)}\right), & \gamma > \kappa, \\ 0, & \gamma = \kappa, \end{cases} \tag{E.11}$$

and

$$B_o(t) \sim \begin{cases} \dfrac{t^\gamma}{\Gamma(1+\gamma)} + O\left(t^\kappa\right), & \gamma < \kappa, \\ -\dfrac{t^\kappa}{\Gamma(1+\kappa)} + O\left(t^{\min(2\kappa,\gamma)}\right), & \gamma > \kappa, \\ 0, & \gamma = \kappa. \end{cases} \tag{E.12}$$

As for Model I, applying (4.37) and (5.7) we find

$$B_n^{\#}(t) \sim -\frac{\mu^2 t^\kappa}{\lambda_n^2 \Gamma(1+\kappa)} + O\left(t^{\min(2\kappa,\gamma+\kappa)}\right), \tag{E.13}$$

$$B_o^{\#}(t) \sim -\frac{\mu^2 L^2 t^\kappa}{6\Gamma(1+\kappa)} + \frac{t^\gamma}{\Gamma(1+\gamma)} + O\left(t^{\min(2\kappa,\gamma+\kappa)}\right). \tag{E.14}$$

Both models. The results from both models for $A_n(t)$ and $B_n(t)$ (or $B_n^{\#}(t)$) using (E.1) (or (E.2)) show that our solutions satisfy the initial condition

$$V(x,0) = \psi(x;\mu) + \sum_{n=0}^{\infty} c_n \Psi_n(x). \tag{E.15}$$

For Model II, this validates the analysis in Appendix A.

E.2. Large *t*.

Model I. For large t we see from (4.11) that $A_n(t)$ decays exponentially to zero, namely,

$$A_n(t) = \mathrm{e}^{-\mu^2 t^\kappa - \lambda_n^2 t^\gamma}. \tag{E.16}$$

To find the asymptotic expressions for $B_n(t)$ we note we can first rewrite (4.14) as

$$B_n(t) = \frac{1}{\lambda_n^2 + \mu^2}\left(A_n(t) - 1\right) + \int_0^t \mathrm{e}^{-\mu^2(t^\kappa - v^\kappa) - \lambda_n^2 (t^\gamma - v^\gamma)} \gamma v^{\gamma-1}\, dv. \tag{E.17}$$

The long time behavior can then be found by applying Laplace's method [21] to the integrals. The temporal behavior of $B_n^{\#}(t)$ can then be obtained via (4.37) and (5.7).

For long times we find for $B_n(t)$ and $B_n^{\#}(t)$ the approximations

$$B_n(t) \sim \begin{cases} -\dfrac{1}{\lambda_n^2 + \mu^2} + \dfrac{\gamma\, t^{-(\kappa-\gamma)}}{\mu^2 \kappa} + O\left(t^{-2(\kappa-\gamma)}\right), & \gamma < \kappa, \\ 0, & \gamma = \kappa, \\ \dfrac{\mu^2}{\lambda_n^2\,(\lambda_n^2 + \mu^2)} - \dfrac{\mu^2 \kappa\, t^{-(\gamma-\kappa)}}{\lambda_n^4\, \gamma} + O\left(t^{-2(\gamma-\kappa)}\right), & \gamma > \kappa, \end{cases} \tag{E.18}$$

and

$$B_n^{\#}(t) \sim \begin{cases} -\dfrac{1}{\lambda_n^2} + \dfrac{\gamma\, t^{-(\kappa-\gamma)}}{\mu^2 \kappa} + O(t^{-2(\kappa-\gamma)}), & \gamma < \kappa, \\ -\dfrac{\mu^2}{\lambda_n^2\,(\lambda_n^2 + \mu^2)}\left(1 - \mathrm{e}^{-\mu^2 t^\kappa - \lambda_n^2 t^\gamma}\right), & \gamma = \kappa, \\ -\dfrac{\mu^2 \kappa\, t^{-(\gamma-\kappa)}}{\lambda_n^4\, \gamma} + \dfrac{\mu^4 \kappa^2\, t^{-2(\gamma-\kappa)}}{\lambda_n^6\, \gamma^2} + O\left(t^{-\min(2\gamma-\kappa, 3(\gamma-\kappa))}\right), & \gamma > \kappa. \end{cases} \tag{E.19}$$

For $B_o(t)$ and $B_o^{\#}(t)$ we can alternatively apply (B.7) to the Mittag–Leffler functions in their respective definitions (4.18) and (4.41). Their respective approximations are then

$$B_o(t) \sim \begin{cases} -\dfrac{1}{\mu^2} + \dfrac{\gamma\, t^{-(\kappa-\gamma)}}{\mu^2 \kappa} + O\left(t^{-(2\kappa-\gamma)}\right) & \text{if } \gamma < \kappa, \\ 0, & \gamma = \kappa, \\ \dfrac{\gamma\, t^{\gamma-\kappa}}{\mu^2 \kappa} - \dfrac{1}{\mu^2} + O\left(t^{-(2\kappa-\gamma)}\right), & \kappa < \gamma < 2\kappa, \\ \dfrac{2\, t^\kappa}{\mu^2} - \dfrac{\mu^2 + 2}{\mu^4} + O\left(\exp\left(-\mu^2 t^\kappa\right)\right), & \gamma = 2\kappa, \\ \dfrac{\gamma\, t^{\gamma-\kappa}}{\mu^2 \kappa} - \left(\dfrac{\gamma}{\kappa} - 1\right)\dfrac{\gamma\, t^{\gamma-2\kappa}}{\mu^4 \kappa} + O\left(t^{-\min(0, 3\kappa-\gamma)}\right), & 2\kappa < \gamma, \end{cases} \tag{E.20}$$

and

$$B_o^{\#}(t) \sim \begin{cases} -\dfrac{L^2}{6} + \dfrac{\gamma\, t^{-(\kappa-\gamma)}}{\mu^2\kappa} + O\left(t^{-(2\kappa-\gamma)}\right) & \text{if } \gamma < \kappa, \\ -\left(\dfrac{L^2}{6} - \dfrac{1}{\mu^2}\right)\left(1 - \mathrm{e}^{-\mu^2 t^\kappa}\right), & \gamma = \kappa, \\ \dfrac{\gamma\, t^{\gamma-\kappa}}{\mu^2\kappa} - \dfrac{L^2}{6} + O\left(t^{-(2\kappa-\gamma)}\right), & \kappa < \gamma < 2\kappa, \\ \dfrac{2\, t^\kappa}{\mu^2} - \left(\dfrac{L^2}{6} + \dfrac{2}{\mu^4}\right) + O\left(\exp\left(-\mu^2 t^\kappa\right)\right), & \gamma = 2\kappa, \\ \dfrac{\gamma\, t^{\gamma-\kappa}}{\mu^2\kappa} - \left(\dfrac{\gamma}{\kappa} - 1\right)\dfrac{\gamma\, t^{\gamma-2\kappa}}{\mu^4\kappa} + O\left(t^{-\min(0,3\kappa-\gamma)}\right), & 2\kappa < \gamma. \end{cases} \tag{E.21}$$

Model II. To determine the long time behavior of the functions $A_n(t)$, $B_n(t)$, and $B_n^{\#}(t)$ we note we can write $A_n(t)$ in two different forms. The first form is as given in (4.25),

$$A_n(t) = \sum_{m=0}^{\infty} \frac{\left(-\mu^2 t^\kappa\right)^m}{m!} E^{(m)}_{\gamma,1+(\kappa-\gamma)m}\left(-\lambda_n^2 t^\gamma\right), \tag{E.22}$$

and the second form is

$$A_n(t) = \sum_{j=0}^{\infty} \frac{\left(-\lambda_n^2 t^\gamma\right)^j}{j!} E^{(j)}_{\kappa,1-(\kappa-\gamma)j}\left(-\mu^2 t^\kappa\right), \tag{E.23}$$

found by using the definition (B.1) and interchanging the order of summation. Applying the asymptotic approximation for the derivative of the Mittag–Leffler function (B.8) to (E.22) and (E.23) we can find asymptotic expansions for $A_n(t)$ to the respective cases $\gamma > \kappa$ and $\gamma < \kappa$. When $\gamma = \kappa$ we can use either form.

The asymptotic expansion for $A_n(t)$ can then be found as (for $\gamma \neq 1$ and $\kappa \neq 1$)

$$A_n(t) \sim \begin{cases} \dfrac{t^{-\kappa}}{\mu^2\,\Gamma(1-\kappa)} - \dfrac{\lambda_n^2\, t^{-2\kappa+\gamma}}{\mu^4\,\Gamma(1-2\kappa+\gamma)} + O(t^{-\min(2\kappa,3\kappa-2\gamma)}), & \gamma < \kappa, \\ \dfrac{t^{-\gamma}}{(\mu^2+\lambda_n^2)\,\Gamma(1-\gamma)} - \dfrac{t^{-2\gamma}}{(\mu^2+\lambda_n^2)^2\,\Gamma(1-2\gamma)} + O(t^{-3\gamma}), & \gamma = \kappa, \\ \dfrac{t^{-\gamma}}{\lambda_n^2\Gamma(1-\gamma)} - \dfrac{\mu^2\, t^{-2\gamma+\kappa}}{\lambda_n^4\,\Gamma(1-2\gamma+\kappa)} + O(t^{-\min(2\gamma,3\gamma-2\kappa)}), & \gamma > \kappa. \end{cases} \tag{E.24}$$

In the case $\lambda_n = 0$ we have, identical to the $\gamma = \kappa$ case but with $\lambda_n = 0$,

$$A_o(t) \sim \frac{t^{-\kappa}}{\mu^2\,\Gamma(1-\kappa)} - \frac{t^{-\kappa}}{\mu^4\,\Gamma(1-2\kappa)} + O\left(t^{-3\kappa}\right). \tag{E.25}$$

The asymptotic approximations for the functions $B_n(t)$ are found by using the appropriate asymptotic expansion for $A_n(t)$ in combination with the definitions (4.27) and (4.28). The asymptotic behavior of $B_n^{\#}(t)$ can then be obtained via (4.37) and (5.7).

The asymptotic approximations for the functions $B_n(t)$, $B_n^{\#}(t)$, $B_o(t)$, and $B_o^{\#}(t)$

are, respectively,

(E.26)
$$B_n(t) \sim \begin{cases} -\dfrac{1}{\lambda_n^2+\mu^2} + \dfrac{t^{-(\kappa-\gamma)}}{\mu^2\,\Gamma\left(1-(\kappa-\gamma)\right)} + O(t^{-\min(\kappa,2(\kappa-\gamma))}), & \gamma<\kappa, \\ 0, & \gamma=\kappa, \\ \dfrac{\mu^2}{\lambda_n^2\,(\lambda_n^2+\mu^2)} - \dfrac{\mu^2 t^{-(\gamma-\kappa)}}{\lambda_n^4\,\Gamma\left(1-(\gamma-\kappa)\right)} + O\left(t^{-\min(\gamma,2(\gamma-\kappa))}\right), & \gamma>\kappa, \end{cases}$$

(E.27)
$$B_n^{\#}(t) \sim \begin{cases} -\dfrac{1}{\lambda_n^2} + \dfrac{t^{-(\kappa-\gamma)}}{\mu^2\,\Gamma\left(1-(\kappa-\gamma)\right)} + O(t^{-\kappa}), & \gamma<\kappa, \\ -\dfrac{\mu^2}{\lambda_n^2\,(\lambda_n^2+\mu^2)} + \dfrac{\mu^2\,t^{-\gamma}}{\lambda_n^2\,(\lambda_n^2+\mu^2)^2\,\Gamma\left(1-\gamma\right)} + O\left(t^{-2\gamma}\right), & \gamma=\kappa, \\ -\dfrac{\mu^2\,t^{-(\gamma-\kappa)}}{\lambda_n^4\,\Gamma\left(1-(\gamma-\kappa)\right)} + \dfrac{\mu^4\,t^{-2(\gamma-\kappa)}}{\lambda_n^6\,\Gamma\left(1-2\,(\gamma-\kappa)\right)} + O\left(t^{-\min(2\gamma-\kappa,3(\gamma-\kappa))}\right), & \gamma>\kappa, \end{cases}$$

(E.28)
$$B_o(t) \sim \begin{cases} -\dfrac{1}{\mu^2} + \dfrac{t^{-(\kappa-\gamma)}}{\mu^2\Gamma\left(1-(\kappa-\gamma)\right)} + O(t^{-\kappa}), & \gamma<\kappa, \\ 0, & \gamma=\kappa, \\ \dfrac{t^{\gamma-\kappa}}{\mu^2\Gamma\left(1+\gamma-\kappa\right)} - \dfrac{1}{\mu^2} + O\left(t^{-(2\kappa-\gamma)}\right), & \kappa<\gamma<2\kappa, \\ \dfrac{t^{\kappa}}{\mu^2\Gamma\left(1+\kappa\right)} - \dfrac{\mu^2+1}{\mu^4} + O\left(t^{-\kappa}\right), & \gamma=2\kappa, \\ \dfrac{t^{\gamma-\kappa}}{\mu^2\Gamma\left(1+\gamma-\kappa\right)} - \dfrac{t^{\gamma-2\kappa}}{\mu^4\Gamma\left(1+\gamma-2\kappa\right)} + O\left(t^{-\min(0,3\kappa-\gamma)}\right), & 2\kappa<\gamma, \end{cases}$$

and

(E.29)
$$B_o^{\#}(t) \sim \begin{cases} -\dfrac{L^2}{6} + \dfrac{t^{-(\kappa-\gamma)}}{\mu^2\Gamma\left(1-(\kappa-\gamma)\right)} + O(t^{-\kappa}), & \gamma<\kappa, \\ -\left(\dfrac{L^2}{6}-\dfrac{1}{\mu^2}\right)\left(1-\dfrac{t^{-\kappa}}{\mu^2\Gamma\left(1-\kappa\right)}\right) + O\left(t^{-2\kappa}\right), & \gamma=\kappa, \\ \dfrac{t^{\gamma-\kappa}}{\mu^2\Gamma\left(1+\gamma-\kappa\right)} - \dfrac{L^2}{6} + O\left(t^{-(2\kappa-\gamma)}\right), & \kappa<\gamma<2\kappa, \\ \dfrac{t^{\kappa}}{\mu^2\Gamma\left(1+\kappa\right)} - \left(\dfrac{L^2}{6}+\dfrac{1}{\mu^4}\right) + O\left(t^{-\kappa}\right), & \gamma=2\kappa, \\ \dfrac{t^{\gamma-\kappa}}{\mu^2\Gamma\left(1+\gamma-\kappa\right)} - \dfrac{t^{\gamma-2\kappa}}{\mu^4\Gamma\left(1+\gamma-2\kappa\right)} + O\left(t^{-\min(0,3\kappa-\gamma)}\right), & 2\kappa<\gamma. \end{cases}$$

Both models. We see from (E.16), (E.24), and (E.25) that for both models $A_n(t)$ decays to zero for any combination of nonzero γ and κ. Considering the behavior of the functions $B_n(t)$ and $B_n^{\#}(t)$ we see different long time behavior of the solutions in (E.1) and (E.2) when $\gamma=\kappa$, $\gamma>\kappa$, and $\gamma<\kappa$. We use the form (E.1) when considering equal exponents and use the other form, (E.2), for the cases $\gamma>\kappa$ and $\gamma<\kappa$.

For the case of equal exponents we use the solution form (E.1) and note that $B_n(t)=0$. Here we see that the potential approaches a steady state, namely,

(E.30) $$V(x,t) \to \psi(x;\mu) \text{ as } t\to\infty.$$

When $\gamma > \kappa$ we find that the long time behavior of the potential is

$$V(x,t) \to \psi(x;0) \text{ as } t \to \infty \tag{E.31}$$

or

$$V(x,t) \sim \frac{d_o X_o(x) \omega_1}{\mu^2} t^{\gamma-\kappa} + O(1) \tag{E.32}$$

when there is a zero eigenvalue present ($\lambda_n = 0$). Here ω_1 is given by γ/κ or $1/\Gamma(1+\gamma-\kappa)$ for Models I and II, respectively.

Finally, if $\gamma < \kappa$, we have, when there is no zero eigenvalue,

$$V(x,t) \sim \psi(x;0) - \sum_{n=1}^{\infty} \frac{d_n \Psi_n(x)}{\lambda_n^2} + O\left(t^{-(\kappa-\gamma)}\right), \tag{E.33}$$

and when there is a zero eigenvalue,

$$V(x,t) \sim \psi_o(x) - \left(\frac{L^2\, d_o \Psi_o(x)}{6} + \sum_{n=1}^{\infty} \frac{d_n \Psi_n(x)}{\lambda_n^2} \right) + O\left(t^{-\omega_3}\right). \tag{E.34}$$

Here ω_3 is $\kappa - \gamma$ or $\max(\kappa-\gamma, \gamma)$ for Models I and II, respectively. These results can be simplified further by noting that both

$$\psi(x;0) - \sum_{n=1}^{\infty} \frac{d_n \Psi_n(x)}{\lambda_n^2} = 0 \tag{E.35}$$

and

$$\psi_o(x) - \left(\frac{L^2\, d_o \Psi_o(x)}{6} + \sum_{n=1}^{\infty} \frac{d_n \Psi_n(x)}{\lambda_n^2} \right) = 0 \tag{E.36}$$

for $0 < x < L$. This can be shown by multiplying by the eigenfunction, $\Psi_n(x)$, and integrating over $0 \le x \le L$, noting that $\psi(x,0)$ and $\psi_o(x)$ satisfy (2.6) and $\Psi_n(x)$ satisfies (2.9). These results suggest, along with (E.33) and (E.34), that if $\gamma < \kappa$, the solution will decay to zero. That is,

$$V(x,t) \sim O\left(t^{-\omega_4}\right) \tag{E.37}$$

with $\omega_4 = \omega_3$ or $\kappa - \gamma$ when there is and is not a zero eigenvalue, respectively.

These results for $\gamma < \kappa$ pairs suggest that both boundary conditions are not satisfied. However, direct evaluation of the boundary conditions using (E.1) or (E.2) shows that they are satisfied for all time! This indicates the presence of boundary layers at one or both ends of the cable.

Appendix F. Verification of solutions. In section 4 of the paper we derived the general solution for Model I (1.17) given by (4.7), (4.11), (4.14), and (4.15), and we derived the general solution for Model II (1.18) given by (4.23), (4.25), (4.29), and (4.30). In this appendix we have verified these solutions by substituting them into the model equations and recovering identities.

F.1. Model I. Consider (1.17) rearranged to bring all terms to the left-hand side:

$$\frac{\partial V}{\partial T} - \gamma T^{\gamma-1}\frac{\partial^2 V}{\partial X^2} + \mu^2\kappa T^{\kappa-1}(V) = 0. \tag{F.1}$$

We will show that

$$V(X,T) = \psi(X;\mu) + \sum_{n=0}^{\infty}\left[c_n A_n(T) + d_n B_n(T)\right]\Psi_n(X) \tag{F.2}$$

satisfies (F.1) with $A_n(T)$ and $B_n(T)$ defined by (4.11), (4.14), and (4.15). Substituting (F.2) and evaluating the derivatives, we find

$$\begin{aligned}\frac{\partial V}{\partial T} - \gamma T^{\gamma-1}\frac{\partial^2 V}{\partial X^2} + \mu^2\kappa T^{\kappa-1}(V) &= \sum_{n=0}^{\infty}\left[c_n\frac{dA_n}{dT} + d_n\frac{dB_n}{dT}\right]\Psi_n(X)\\ &\quad - \gamma T^{\gamma-1}\left(\frac{d^2\psi(X;\mu)}{dX^2} + \sum_{n=0}^{\infty}\left[c_n A_n(T) + d_n B_n(T)\right]\frac{d^2\Psi_n(X)}{dX^2}\right)\\ &\quad + \mu^2\kappa T^{\kappa-1}\left(\psi(X;\mu) + \sum_{n=0}^{\infty}\left[c_n A_n(T) + d_n B_n(T)\right]\Psi_n(X)\right),\end{aligned} \tag{F.3}$$

which simplifies with the help of (2.5) and (2.12) to

$$\begin{aligned}\frac{\partial V}{\partial T} - \gamma T^{\gamma-1}\frac{\partial^2 V}{\partial X^2} + \mu^2\kappa T^{\kappa-1}(V) &= -\mu^2\left(\gamma T^{\gamma-1} - \kappa T^{\kappa-1}\right)\psi(X;\mu)\\ &\quad + \sum_{n=0}^{\infty} c_n\left[\frac{dA_n}{dT} + \left(\lambda_n^2\gamma T^{\gamma-1} + \mu^2\kappa T^{\kappa-1}\right)A_n(T)\right]\Psi_n(X)\\ &\quad + \sum_{n=0}^{\infty} d_n\left[\frac{dB_n}{dT} + \left(\lambda_n^2\gamma T^{\gamma-1} + \mu^2\kappa T^{\kappa-1}\right)B_n(T)\right]\Psi_n(X).\end{aligned} \tag{F.4}$$

Now using $A_n(T)$ from (4.11), we see that

$$\begin{aligned}&\frac{dA_n}{dT} + \left(\lambda_n^2\gamma T^{\gamma-1} + \mu^2\kappa T^{\kappa-1}\right)A_n(T)\\ &\quad = \frac{d}{dT}\left(\mathrm{e}^{-\mu^2 T^{\kappa} - \lambda_n^2 T^{\gamma}}\right) + \left(\lambda_n^2\gamma T^{\gamma-1} + \mu^2\kappa T^{\kappa-1}\right)\mathrm{e}^{-\mu^2 T^{\kappa} - \lambda_n^2 T^{\gamma}}\\ &\quad = -\left(\lambda_n^2\gamma T^{\gamma-1} + \mu^2\kappa T^{\kappa-1}\right)\mathrm{e}^{-\mu^2 T^{\kappa} - \lambda_n^2 T^{\gamma}}\\ &\qquad + \left(\lambda_n^2\gamma T^{\gamma-1} + \mu^2\kappa T^{\kappa-1}\right)\mathrm{e}^{-\mu^2 T^{\kappa} - \lambda_n^2 T^{\gamma}}\\ &\quad = 0.\end{aligned} \tag{F.5}$$

Using (4.9) we also have

$$\begin{aligned}&\frac{dB_n}{dT} + \left(\lambda_n^2\gamma T^{\gamma-1} + \mu^2\kappa T^{\kappa-1}\right)B_n(T)\\ &\quad = \mathrm{e}^{-\mu^2 T^{\kappa}}\gamma T^{\gamma-1}\left[\frac{dB_n^*(T^{\gamma})}{dT} + \lambda_n^2 B_n^*(T^{\gamma})\right].\end{aligned} \tag{F.6}$$

To simplify further we first note that we can rewrite (4.12) as

(F.7)
$$B_n^*(T) = \frac{1}{\lambda_n^2+\mu^2}\left(A_n^*(T) - P_\theta(T)\right) + T\sum_{m=0}^{\infty}\frac{\left(\mu^2 T^\theta\right)^m}{m!}\Gamma\left(1+\theta m\right)E_{1,2+\theta m}(-\lambda_n^2 T),$$

an expression that remains valid when λ_n is zero. We now have

$$\frac{dB_n^*(T)}{dT} + \lambda_n^2 B_n^* = \frac{1}{\lambda_n^2+\mu^2}\left(-\lambda_n^2 A_n^*(T) - \mu^2\theta T^{\theta-1}P_\theta(T)\right) + \frac{\lambda_n^2}{\lambda_n^2+\mu^2}\left(A_n^*(T) - P_\theta(T)\right)$$
$$+\sum_{m=0}^{\infty}\frac{\left(\mu^2 t^\theta\right)^m}{m!}\Gamma\left(1+\theta m\right)\left(E_{1,1+\theta m}(-\lambda_n^2 T) + \lambda_n^2 T E_{1,2+\theta m}(-\lambda_n^2 T)\right).$$

(F.8)

This can be simplified further using the identity (cf. (B.3))

$$E_{1,1+\theta m}(z) - zE_{1,2+\theta m}(z) = \frac{1}{\Gamma\left(1+\theta m\right)} \tag{F.9}$$

with $z = -\lambda_n^2 T$ to give

$$\frac{dB_n^*(T)}{dT} + \lambda_n^2 B_n^* = -\frac{P_\theta(T)}{\lambda_n^2+\mu^2}\left(\lambda_n^2 + \mu^2\theta T^{\theta-1}\right) + \sum_{m=0}^{\infty}\frac{\left(\mu^2 T^\theta\right)^m}{m!}$$
$$= \frac{\mu^2 P_\theta(T)}{\lambda_n^2+\mu^2}\left(1 - \mu^2\theta T^{\theta-1}\right). \tag{F.10}$$

Using this result in (F.6), we find

$$\frac{dB_n}{dT} + \left(\lambda_n^2\gamma T^{\gamma-1} + \mu^2\kappa T^{\kappa-1}\right)B_n(T) = \frac{\mu^2}{\lambda_n^2+\mu^2}\left(\gamma T^{\gamma-1} - \kappa T^{\kappa-1}\right). \tag{F.11}$$

Finally, using (F.5) and (F.11) in (F.4), we find

$$\frac{\partial V}{\partial T} - \gamma T^{\gamma-1}\frac{\partial^2 V}{\partial X^2} + \mu^2\kappa T^{\kappa-1}\left(V\right)$$
$$= \mu^2\left(\gamma T^{\gamma-1} - \kappa T^{\kappa-1}\right)\left[\sum_{n=0}^{\infty}\frac{d_n}{\lambda_n^2+\mu^2}\Psi_n(X) - \psi(X;\mu)\right]. \tag{F.12}$$

The term in the brackets [ ] is zero for $0 < X < L$, which can be seen by taking the limit $\lambda \to \infty$ in (4.1). In general, $\psi(X;\mu)$ and $\Psi_n(X)$ satisfy different boundary conditions (given by (2.5) and (2.12), respectively) so that the term in brackets [ ] is not zero at $X = 0$ or at $X = L$. Thus (4.7) (with (4.11), (4.14), and (4.15)) is the solution of (1.17) for Model I on the finite domain $0 < X < L$.

F.2. Model II. Consider (1.18) again rearranged to bring all terms to the left-hand side:

$$\frac{\partial V}{\partial t} - \frac{\partial^{1-\gamma}}{\partial t^{1-\gamma}}\left(\frac{\partial^2 V}{\partial x^2}\right) + \mu^2\frac{\partial^{1-\kappa}}{\partial t^{1-\kappa}}\left(V\right) = 0. \tag{F.13}$$

We will show that

$$V(X,T) = \psi(X;\mu) + \sum_{n=0}^{\infty}\left[c_n A_n(T) + d_n B_n(T)\right]\Psi_n(X) \tag{F.14}$$

satisfies (F.13) with $A_n(T)$ and $B_n(T)$ defined by (4.25), (4.29), and (4.30).

Substituting (F.14) and evaluating the derivatives, we find

$$\begin{aligned}(\text{F.15})\quad \frac{\partial V}{\partial T}-\frac{\partial^{1-\gamma}}{\partial t^{1-\gamma}}\left(\frac{\partial^2 V}{\partial X^2}\right)+\mu^2\frac{\partial^{1-\kappa}}{\partial t^{1-\kappa}}(V)&=\sum_{n=0}^{\infty}\left[c_n\frac{dA_n}{dT}+d_n\frac{dB_n}{dT}\right]\Psi_n(X)\\ -\left(\frac{T^{\gamma-1}}{\Gamma(\gamma)}\frac{d^2\psi(X;\mu)}{dX^2}+\sum_{n=0}^{\infty}\left[c_n\frac{d^{1-\gamma}A_n}{dT^{1-\gamma}}+d_n\frac{d^{1-\gamma}B_n}{dT^{1-\gamma}}\right]\frac{d^2\Psi_n(X)}{dX^2}\right)&\\ +\mu^2\left(\frac{T^{\kappa-1}}{\Gamma(\kappa)}\psi(X;\mu)+\sum_{n=0}^{\infty}\left[c_n\frac{d^{1-\gamma}A_n}{dT^{1-\gamma}}+d_n\frac{d^{1-\gamma}B_n}{dT^{1-\gamma}}\right]\Psi_n(X)\right),&\end{aligned}$$

where we have used the fractional derivative of a constant given in (5.15). Now simplifying with the help of (2.5) and (2.12) we find

$$\begin{aligned}(\text{F.16})\quad \frac{\partial V}{\partial T}-\frac{\partial^{1-\gamma}}{\partial t^{1-\gamma}}\left(\frac{\partial^2 V}{\partial X^2}\right)+\mu^2\frac{\partial^{1-\kappa}}{\partial t^{1-\kappa}}(V)&=-\mu^2\left(\frac{T^{\gamma-1}}{\Gamma(\gamma)}-\frac{T^{\kappa-1}}{\Gamma(\kappa)}\right)\psi(X;\mu)\\ +\sum_{n=0}^{\infty}c_n\left[\frac{dA_n}{dT}+\lambda_n^2\frac{d^{1-\gamma}A_n}{dT^{1-\gamma}}+\mu^2\frac{d^{1-\kappa}A_n}{dT^{1-\kappa}}\right]\Psi_n(X)&\\ +\sum_{n=0}^{\infty}d_n\left[\frac{dB_n}{dT}+\lambda_n^2\frac{d^{1-\gamma}B_n}{dT^{1-\gamma}}+\mu^2\frac{d^{1-\kappa}B_n}{dT^{1-\kappa}}\right]\Psi_n(X).&\end{aligned}$$

We can simplify the above using Laplace transform methods. First consider

$$\begin{aligned}\mathcal{L}\left\{\frac{dA_n}{dT}+\lambda_n^2\frac{d^{1-\gamma}A_n}{dT^{1-\gamma}}+\mu^2\frac{d^{1-\kappa}A_n}{dt^{1-\kappa}}\right\}(s)&=s\widehat{A}_n(s)-A_n(0)+\left(\lambda_n^2 s^{1-\gamma}+\mu^2 s^{1-\kappa}\right)\widehat{A}_n(s)\\ &=\left(s+\lambda_n^2 s^{1-\gamma}+\mu^2 s^{1-\kappa}\right)\widehat{A}_n(s)-1,\end{aligned}\qquad(\text{F.17})$$

where we have used the identity $A_n(0)=1$. The Laplace transform of A_n is given by (cf. (4.20))

$$\widehat{A}_n(s)=\frac{1}{s+\lambda_n^2 s^{1-\gamma}+\mu^2 s^{1-\kappa}};\qquad(\text{F.18})$$

then we find that (F.17) is zero, and so after inverting,

$$\frac{dA_n}{dT}+\lambda_n^2\frac{d^{1-\gamma}A_n}{dT^{1-\gamma}}+\mu^2\frac{d^{1-\kappa}A_n}{dT^{1-\kappa}}=0.\qquad(\text{F.19})$$

Now consider

(F.20)

$$\begin{aligned}\mathcal{L}\left\{\frac{dB_n}{dT}+\lambda_n^2\frac{d^{1-\gamma}B_n}{dT^{1-\gamma}}+\mu^2\frac{d^{1-\kappa}B_n}{dT^{1-\kappa}}\right\}(s)&=s\widehat{B}_n(s)-B_n(0)+\left(\lambda_n^2 s^{1-\gamma}+\mu^2 s^{1-\kappa}\right)\widehat{B}_n(s)\\ &=\left(s+\lambda_n^2 s^{1-\gamma}+\mu^2 s^{1-\kappa}\right)\widehat{B}_n(s),\end{aligned}$$

where we have used the identity $B_n(0)=0$.

The Laplace transform of $B_n(T)$ is given by (cf. (4.21))

(F.21)

$$\widehat{B}_n(s)=\frac{\mu^2}{\lambda_n^2+\mu^2}\left(s^{-\gamma}-s^{-\kappa}\right)\widehat{A}_n(s)=\left(\frac{\mu^2}{\lambda_n^2+\mu^2}\right)\left(\frac{s^{-\gamma}-s^{-\kappa}}{s+\lambda_n^2 s^{1-\gamma}+\mu^2 s^{1-\kappa}}\right).$$

After substituting in (F.21), we have

$$\mathcal{L}\left\{\frac{dB_n}{dT}+\lambda_n^2\frac{d^{1-\gamma}B_n}{dT^{1-\gamma}}+\mu^2\frac{d^{1-\kappa}B_n}{dT^{1-\kappa}}\right\}(s)=\frac{\mu^2\left(s^{-\gamma}-s^{-\kappa}\right)}{\lambda_n^2+\mu^2}, \tag{F.22}$$

and then after inverting,

$$\frac{dB_n}{dT}+\lambda_n^2\frac{d^{1-\gamma}B_n}{dT^{1-\gamma}}+\mu^2\frac{d^{1-\kappa}B_n}{dT^{1-\kappa}}=\frac{\mu^2}{\lambda_n^2+\mu^2}\left(\frac{T^{\gamma-1}}{\Gamma(1-\gamma)}-\frac{T^{\kappa-1}}{\Gamma(1-\kappa)}\right). \tag{F.23}$$

Now using (F.19) and (F.23) in (F.16), we find

$$\begin{aligned}\frac{\partial V}{\partial T}-\frac{\partial^{1-\gamma}}{\partial t^{1-\gamma}}\left(\frac{\partial^2 V}{\partial X^2}\right)+\mu^2\frac{\partial^{1-\kappa}}{\partial t^{1-\kappa}}(V)\\ =\mu^2\left(\frac{T^{\gamma-1}}{\Gamma(1-\gamma)}-\frac{T^{\kappa-1}}{\Gamma(1-\kappa)}\right)\left[\sum_{n=0}^{\infty}\frac{d_n}{\lambda_n^2+\mu^2}\Psi_n(X)-\psi(X;\mu)\right].\end{aligned} \tag{F.24}$$

The term in the brackets [ ] is again zero for $0<X<L$, which can be seen by taking the limit $\lambda\to\infty$ in (4.1). In general, $\psi(X;\mu)$ and $\Psi_n(X)$ satisfy different boundary conditions (given by (2.5) and (2.12), respectively), and the term in brackets [ ] is not zero at $X=0$ or at $X=L$. Thus (4.23) (along with (4.25), (4.29), and (4.30)) is the solution of (1.18) for Model II on the finite domain $0<X<L$.

REFERENCES

[1] M. Abramowitz and I. A. Stegun, eds., *Handbook of Mathematical Functions with Formulas, Graphs, and Mathematical Tables*, 10th ed., Appl. Math. Ser. 55, U.S. Department of Commerce, Washington, DC, 1972.

[2] D. S. Banks and C. Fradin, *Anomalous diffusion of proteins due to molecular crowding*, Biophys. J., 89 (2005), pp. 2960–2971.

[3] D. H. Bhatt, S. Zhang, and W.-B. Gan, *Dendritic spine dynamics*, Annual Review of Physiology, 71 (2009), pp. 261–282.

[4] B. L. J. Braaksma, *Asymptotic expansions and analytic continuations for a class of Barnes-integrals*, Compos. Math., 15 (1963), pp. 239–341.

[5] E. B. Brown, E. S. Wu, W. Zipfel, and W. W. Webb, *Measurement of molecular diffusion in solution by multiphoton fluorescence photobleaching recovery*, Biophys. J., 77 (1999), pp. 2837–2849.

[6] E. Buckwar and Y. Luchko, *Invariance of a partial differential equation of fractional order under the Lie group of scaling transformations*, J. Math. Anal. Appl., 227 (1998), pp. 81–97.

[7] J. D. Eaves and D. R. Reichman, *The subdiffusive targetting problem*, J. Phys. Chem. B, 112 (2008), pp. 4283–4289.

[8] T. J. Feder, I. Brust-Mascher, J. P. Slattery, B. Baird, and W. W. Webb, *Constrained diffusion or immobile fraction on cell surfaces: A new interpretation*, Biophys. J., 70 (1996), pp. 2767–2773.

[9] S. Fedotov and V. Méndez, *Non-Markovian model for transport and reactions of particles in spiny dendrites*, Phys. Rev. Lett., 101 (2008), 218102.

[10] S. Furini, F. Zerbetto, and S. Cavalcanti, *Application of the Poisson-Nernst-Planck theory with space dependent diffusion coefficients to kcsa*, Biophys. J., 91 (2006), pp. 3162–3169.

[11] M. Gabso, E. Neher, and M. E. Spira, *Low mobility of Ca^{2+} buffers in axons of cultured aplysia neurons*, Neuron, 18 (1997), pp. 473–481.

[12] D. S. Grebenkov, *Subdiffusion in a bounded domain with a partially absorbing-reflecting boundary*, Phys. Rev. E, 81 (2010), 021128.

[13] B. I. Henry, T. A. M. Langlands, and S. L. Wearne, *Anomalous diffusion with linear reaction kinetics: From continuous time random walks to fractional reaction-diffusion equations*, Phys. Rev. E, 74 (2006), 031116.

[14] B. I. Henry, T. A. M. Langlands, and S. L. Wearne, *Fractional cable model for spiny neuronal dendrites*, Phys. Rev. Lett., 100 (2008), 128103.

[15] C. Koch, *Biophysics of Computation: Information Processing in Single Neurons*, Computational Neuroscience Series, Oxford University Press, New York, 2004.
[16] T. A. M. Langlands, *Solution of a modified fractional diffusion equation*, Phys. A, 367 (2006), pp. 136–144.
[17] T. A. M. Langlands, B. I. Henry, and S. L. Wearne, *Fractional cable equation models for anomalous electrodiffusion in nerve cells: Infinite domain solutions*, J. Math. Biol., 59 (2009), pp. 761–808.
[18] F. Liu, Q. Yang, and I. Turner, *Two new implicit numerical methods for the fractional cable equation*, J. Comput. Nonlinear Dynam., 6 (2011), 011009.
[19] R. Metzler and J. Klafter, *The random walk's guide to anomalous diffusion: A fractional dynamics approach*, Phys. Rep., 339 (2000), pp. 1–77.
[20] E. Montroll and G. Weiss, *Random walks on lattices* II, J. Math. Phys., 6 (1965), p. 167.
[21] J. D. Murray, *Asymptotic Analysis*, Oxford University Press, Glasgow, 1974.
[22] K. B. Oldham and J. Spanier, *The Fractional Calculus: Theory and Applications of Differentiation and Integration to Arbitrary Order*, Math. Sci. Engrg. 111, Academic Press, New York, London, 1974.
[23] R. B. Paris, *Exponential asymptotics of the Mittag-Leffler function*, Proc. R. Soc. Lond. A, 458 (2002), pp. 3041–3052.
[24] I. Podlubny, *Fractional Differential Equations*, Math. Sci. Engrg. 198, Academic Press, New York, London, 1999.
[25] N. Qian and T. J. Sejnowski, *An electro-diffusion model for computing membrane potentials and ionic concentrations in branching dendrites, spines and axons*, Biol. Cybernet., 62 (1989), pp. 1–15.
[26] W. Rall, *Core conductor theory and cable properties of neurons*, in Handbook of Physiology: The Nervous System, Vol. 1, R. Poeter, ed., American Physiological Society, Bethesda, MD, 1977, pp. 39–97.
[27] A. M. Reynolds, *On the anomalous diffusion characteristics of membrane bound proteins*, Phys. Lett. A, 342 (2005), pp. 439–442.
[28] F. Santamaria, S. Wils, E. De Schutter, and G. J. Augustine, *Anomalous diffusion in Purkinje cell dendrites caused by spines*, Neuron, 52 (2006), pp. 635–648.
[29] M. J. Saxton, *Anomalous diffusion due to obstacles: A Monte Carlo study*, Biophys. J., 66 (1994), pp. 394–401.
[30] M. J. Saxton, *Anomalous diffusion due to binding: A Monte Carlo study*, Biophys. J., 70 (1996), pp. 1250–1262.
[31] M. J. Saxton, *Anomalous subdiffusion in fluorescence photobleaching recovery: A Monte Carlo study*, Biophys. J., 81 (2001), pp. 2226–2240.
[32] S. Schnell and T. E. Turner, *Reaction kinetics in intracellular environments with macromolecular crowding: Simulations and rate laws*, Prog. Biophys. Mol. Biol., 85 (2004), pp. 235–260.
[33] E. D. Sheets, G. M. Lee, R. Simson, and K. Jacobson, *Transient confinement of a glycosylphosphatidylinositol-anchored protein in the plasma membrane*, Biochem., 36 (1997), pp. 12449–12458.
[34] R. Simson, B. Yang, S. E. Moore, P. Doherty, F. S. Walsh, and K. A. Jacobson, *Structural mosaicism on the submicron scale in the plasma membrane*, Biophys. J., 74 (1998), pp. 297–308.
[35] P. R. Smith, I. E. G. Morrison, K. M. Wilson, N. Fernandez, and R. J. Cherry, *Anomalous diffusion of major histocompatability complex class I molecules on HeLa cells determined by single particle tracking*, Biophys. J., 76 (1999), pp. 3331–3344.
[36] H. C. Tuckwell, *Introduction to Theoretical Neurobiology, Vol.* 1, Cambridge University Press, Sydney, 1988.
[37] M. Wachsmuth, T. Weidemann, G. Müller, U. W. Hoffmann-Rohrer, T. A. Knoch, W. Waldeck, and J. Langowski, *Analyzing intracellular binding and diffusion with continuous fluorescence photobleaching*, Biophys. J., 84 (2003), pp. 3353–3363.
[38] K. G. Wang, *Long-range correlation-effects, generalized Brownian-motion and anomalous diffusion*, J. Phys. A, 27 (1994), pp. 3655–3661.
[39] K. G. Wang and C. W. Lung, *Long-time correlation-effects and fractal Brownian-motion*, Phys. Lett. A, 151 (1990), pp. 119–121.
[40] M. Weiss, M. Elsner, F. Kartberg, and T. Nilsson, *Anomalous subdiffusion is a measure for cytoplasmic crowding in living cells*, Biophys. J., 87 (2004), pp. 3518–3524.
[41] R. Wong and Y.-Q. Zhao, *Exponential asymptotics of the Mittag-Leffler function*, Constr. Approx., 18 (2002), pp. 355–385.